A CIRCULARLY SYMMETRIC PRIMITIVE EQUATION MODEL OF TROPICAL CYCLONE DEVELOPMENT CONTAINING AN EXPLICIT WATER VAPOR CYCLE

STANLEY L. ROSENTHAL

National Hurricane Research Laboratory, ESSA, Miami, Fla.

ABSTRACT

The tropical cyclone model described in previous reports is extended to include an explicit water vapor cycle. Results of experiments that examine effects due to initial humidity conditions, radial resolution, and the finite-difference scheme are discussed. Growth to the mature stage is more rapid in the moist environment, but peak intensity is not strongly affected by the initial moisture content. Rainfall rates are quite reasonable, and nonconvective precipitation is found to be a significant proportion of the total rainfall, in agreement with recent empirical results. Experiments with upstream differencing yield more realistic solutions than do experiments with centered differences. This surprising result is discussed in detail.

1. INTRODUCTION

Our circularly symmetric tropical cyclone model (Rosenthal 1969a, 1969b) has been extended to include an explicit calculation of the humidity content of the free atmosphere. The old version[1] of the model could only simulate cumulus convection that originated in the Ekman layer. The new model is able to simulate convection originating at higher levels. Nonconvective precipitation is also simulated and, in agreement with recent empirical results obtained by Hawkins and Rubsam (1968), makes a substantial contribution to the total precipitation.

Examination of the effect of the initial humidity distribution on tropical cyclone development indicates that the mature stage is reached more rapidly in a moist environment. However, the ultimate intensity of the storm does not appear to be strongly influenced.

The adjustments of macroscale humidity and temperature that are intended to simulate the effects of cumulus convection are described in section 2. Section 3 gives the equations for the macroscale water vapor budget. In section 4, we derive a parametric representation of the vertical

transport of horizontal momentum by cumulus scale eddies. Section 5 gives a fairly complete review of the dynamic aspects of the model. In section 6, the results of a benchmark experiment (experiment W1) are presented. This experiment is conducted with 10-km radial resolution, upstream differencing, and a selection of friction and viscosity coefficients that provide a "good" solution based on the author's intuitive concepts of hurricane structure and dynamics. For computational economy, the remaining experiments are conducted with 20-km radial resolution. For isolating effects due solely to resolution, section 7 describes an experiment (experiment W2) identical to W1 in all respects except radial resolution, which is 20 km. Section 8 describes the experiment designed to study the effects of the initial moisture distribution, the results of which have already been summarized above. In section 9, we discuss the results of a number of trial and error experiments that were useful in the design of experiments W1 and W2. Section 10 reviews the main conclusions of the paper.

In comparison to the models devised by Ooyama (1969) and Yamasaki (1968b), our model seems to provide substantial improvement in certain areas while, perhaps, making sacrifices elsewhere. Ooyama's model uses the gradient wind assumption and carries horizontal velocity at three levels in the vertical. Temperature is represented only at an upper level and in the Ekman layer. No allowance for the vertical variation of static stability is provided; water vapor content is predicted only in the boundary layer. Neither nonconvective precipitation nor convective precipitation from convective elements originating above the surface boundary layer is included.

In contrast, our model represents all variables at seven levels, uses the primitive equations, and, as already noted, explicitly predicts water vapor content, nonconvective precipitation, and multilevel convection. Ooyama, however, uses superior finite-difference techniques, finer radial resolution, a computational domain more than twice as large as ours, and makes an explicit prediction of air-sea exchanges of sensible and latent heat. The latter are treated rather pragmatically in the calculations reported on here.

---

[1] The old version is called the "old model"; hereafter, the new version is referred to as the "new model."

Yamasaki (1968b) provides for 13 levels in the vertical and uses the primitive equations. His model, however, contains neither an explicit water vapor cycle, the effects of multilevel convection, nor an explicit treatment of nonconvective precipitation. Yamasaki uses the upstream method for advection terms and variable radial resolution; his *smallest* grid increment is 20 km. His calculations, therefore, should be expected to have substantially more truncation error than our experiments with a fixed resolution of 10 km and somewhat more truncation error than our calculations with a fixed resolution of 20 km. On the other hand, the radial extent of Yamasaki's computational domain is about five times greater than ours. Yamasaki demands the "cloud" equivalent potential temperatures to be constant in the horizontal and with time. In our model, these are allowed to vary as they will according to the scheme developed in sections 2 and 3. Yamasaki's paper (1968b) provides no information concerning the rainfall rates yielded by his model.

The storm structure developed by Yamasaki's model is generally quite realistic. However, horizontal temperature gradients in the lower troposphere appear to be unrealistically large, and the elevation of the greatest temperature anomaly is too low. Our model yields better results in this area. On the other hand, Yamasaki obtains a better vertical profile of radial motion in the upper tropospheric outflow layer.

The following symbols are used:

C_D drag coefficient,
c_p specific heat of air at constant pressure,
f Coriolis parameter,
g acceleration of gravity,
K_M^z kinematic coefficient of eddy viscosity for vertical mixing,
K_M^H kinematic coefficient of eddy viscosity for lateral mixing,
K_T^z kinematic coefficient of eddy diffusivity for vertical mixing of heat,
K_T^H kinematic coefficient of eddy diffusivity for lateral mixing of heat,
K_W^z kinematic coefficient of eddy diffusivity for vertical mixing of water vapor,
K_W^H kinematic coefficient of eddy diffusivity for lateral mixing of water vapor,
L latent heat of evaporation,
M relative angular momentum,
p pressure,
p_0 1000 mb,
q specific humidity,
R specific gas constant for air,
r radius,
T absolute temperature,
t time,
u radial velocity,
$\mathbf{V}$ horizontal vector wind,
v tangential velocity,
w vertical velocity,
z geometric height above mean sea level,
Δr radial increment,

Δt time increment,
θ potential temperature,
θ_E equivalent potential temperature,
ρ air density,
$\bar{\rho}$ standard air density,
ϕ $c_p(p/p_0)^{R/c_p}$, and
ϕ_1 ϕ at level one.

2. CONVECTIVE ADJUSTMENTS OF MACROSCALE TEMPERATURE AND HUMIDITY

This discussion assumes that the reader will make repeated reference to figure 1. We consider a layer of the conditionally unstable lower tropical troposphere centered at a reference level z_β. We assume the roots of an organized system of cumulonimbi to be within the layer. We further assume that the cumulonimbi transport upward and condense $\delta_\beta E$ mass units of water vapor per unit area in some period of time. Part of the condensate reevaporates and enriches the macroscale humidity as the clouds mix with their environment. The remaining condensate falls from the atmosphere as rain. The latent heat released during the formation of this portion of the condensate is assumed available for increasing the macroscale temperature.

The convection therefore produces adjustments in the macroscale humidity and temperature at levels above z_β and below the cloud tops (z_β^{top}). These adjustments are assumed to obey the energy budget

$$\int_{z_\beta}^{z_\beta^{top}} \rho\{c_p\Delta_\beta T(z)+L\Delta_\beta q(z)\}dz=L\delta_\beta E \qquad (1)$$

where $\Delta_\beta T(z)$ and $\Delta_\beta q(z)$ are the macroscale changes of temperature and specific humidity at level z produced by convection originating at level z_β.

We assume (see Rosenthal 1969a for justification) that the convective adjustments are such that the macroscale temperature and equivalent potential temperature tend toward vertical profiles appropriate to parcel ascent from z_β (dry adiabatic lifting to the lifting condensational level followed by pseudoadiabatic ascent to z_β^{top}). Following Kuo (1965), z_β^{top} is taken as the height at which the appropriate pseudoadiabat intersects the macroscale sounding after an intervening layer in which the pseudoadiabat is warmer than the macroscale. Denote this level by z_β^*, $z_\beta^{top}=z_\beta^*$. Now let

$$_\beta\theta_E^c\equiv\theta_E(z_\beta) \qquad (2)$$

be the equivalent potential temperature of a parcel rising from z_β and let

$$T_\beta^c\equiv T^c(z, z_\beta) \qquad (3)$$

be the temperature of the parcel when it reaches level z ($z_\beta\leq z\leq z_\beta^*$). We take

$$\Delta_\beta\theta_E(z)\equiv\Delta_\beta\theta_E=[_\beta\theta_E^c-\theta_E(z)]\delta_\beta\nu$$

and

$$\Delta_\beta T(z)\equiv\Delta_\beta T=[T_\beta^c-T(z)]\delta_\beta\nu \qquad (4)$$

for $z_\beta\leq z\leq z_\beta^*$. The $\theta_E(z)$ and $T(z)$ are the macroscale equivalent potential temperature and temperature at level z. The proportionality factor, $\delta_\beta\nu$, is calculated as
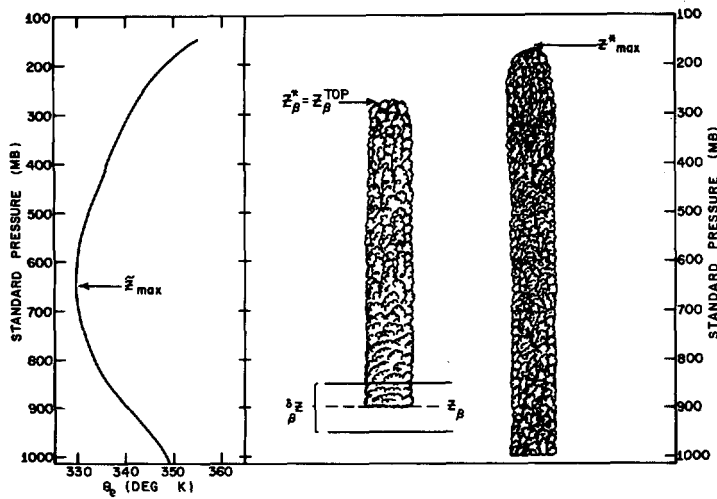
FIGURE 1.—Vertical distribution of equivalent potential temperature for the mean tropical atmosphere (Hebert and Jordan 1959) and model clouds for the convective adjustment. See section 2 for details.

described below. In the event that the right-hand sides of the relationships (4) are zero or negative, the convective adjustments were taken as zero. Following Kuo (1965), $\delta_\beta \nu$ is assumed independent of height and is obtained from the energy budget (1) in a manner to be described later.

We consider short time periods so that the convective adjustments are small and make use of the relationship

$$\theta_E = \theta e^{Lq/c_p T}. \qquad (5)$$

We may then write

$$\frac{\Delta_\beta \theta_E}{\theta_E} \approx \frac{\Delta_\beta T}{T} + \frac{L}{c_p T} \Delta_\beta q. \qquad (6)$$

By use of (3), (4), (5), and (6), we obtain for any reasonable conditions of temperature and humidity

$$\Delta_\beta q \approx (q_\beta^c - q)\delta_\beta \nu. \qquad (7)$$

As in the case of (4), if the right-hand side of (7) is negative or zero, the adjustment is taken as zero. The adjustment relationships (4) and (7) are similar to those given by Kuo (1965).

From (1), (4), and (7),

$$\frac{\delta_\beta \nu}{\delta_\beta E} = \frac{L}{\int_{z_\beta}^{z_\beta^*} \rho\{c_p(T_\beta^c - T) + L(q_\beta^c - q)\}dz}, \quad z_\beta^* \geq z \geq z_\beta,$$

$$\frac{\delta_\beta \nu}{\delta_\beta E} = 0, \quad z < z_\beta \text{ or } z > z_\beta^*. \qquad (8)$$

Now let the conditionally unstable portion of the lower tropical troposphere be divided into n thin layers all of which contain cumulonimbi roots and behave as the layer described above. For the sake of brevity, it is assumed that conditional instability is found from $z = 0$ to $z = \tilde{z}_{max}$ without intervening stable layers. It is also assumed that each of these layers has a water vapor supply sufficient to support moist convection. These assumptions (not made

in the numerical model) avoid tedious repetition in the mathematical manipulations.

The net temperature change at a level z due to the convection from the n layers is then

$$\Delta T(z) = \sum_{\beta=1}^{m} \Delta_\beta T(z) = \sum_{\beta=1}^{m} \{T_\beta^c(z) - T(z)\}\delta_\beta \nu, \quad z \leq \tilde{z}_{max} \qquad (9)$$

where m is the number of convective layers below z and $m \leq n$. Also,

$$\Delta T(z) = \sum_{\beta=1}^{n} \{T_\beta^c(z) - T(z)\}\delta_\beta \nu, \quad \tilde{z}_{max} < z \leq z_{max}^* \qquad (10)$$

where z_{max}^* is the highest cloud top. Equations (9) and (10) are somewhat similar to those recently suggested by Estoque (1968) for convection originating from multiple layers. From (9) and (10),

$$\Delta T(z) = \sum_{\beta=1}^{n \text{ or } m} \{T_\beta^c(z) - T(z)\} \frac{\delta_\beta \nu}{\delta_\beta E} \frac{\delta_\beta E}{\delta_\beta z} \delta_\beta z \qquad (11)$$

where $\delta_\beta z$ is the thickness of the βth convective layer. The analogous equation for humidity is

$$\Delta q(z) = \sum_{\beta=1}^{n \text{ or } m} \{q_\beta^c(z) - q(z)\} \frac{\delta_\beta \nu}{\delta_\beta E} \frac{\delta_\beta E}{\delta_\beta z} \delta_\beta z. \qquad (12)$$

The macroscale heating per unit time and area may be written

$$\dot{Q}(z) = \lim_{\Delta t \to 0} \left\{ \frac{c_p \Delta T(z)}{\Delta t} \right\}, \qquad (13)$$

and the convective precipitation rate for a column of unit area (mass of water per unit time) is

$$\dot{\pi} = \int_0^\infty \frac{\rho \dot{Q}}{L} dz. \qquad (14)$$

The calculation of $\delta_\beta \nu$ and $\delta_\beta E$ is described in the next section.

3. WATER VAPOR BUDGET

In the absence of phase changes, we take the macroscale specific humidity to be governed by

$$\bar{\rho} \frac{\partial q}{\partial t} = -\frac{1}{r} \frac{\partial \bar{\rho} u q r}{\partial r} - \frac{\partial \bar{\rho} w q}{\partial z} + \bar{\rho} \frac{K_W^H}{r} \frac{\partial}{\partial r} \left(r \frac{\partial q}{\partial r} \right) + \frac{\partial}{\partial z} \left(\bar{\rho} K_W^z \frac{\partial q}{\partial z} \right). \qquad (15)$$

Consider a vertical column extending from the sea surface to the top of the atmosphere. Except for transfers across the upper and lower boundaries of the column, the second and fourth terms on the right-hand side of equation (15) represent vertical redistributions of vapor that do not affect the vapor content of the column as a whole. The contribution to the vertically integrated time rate of change of humidity by processes in the reference layer $\delta_\beta z$ (fig. 1) may then be written as

$$S(z_\beta) = \left\{ \frac{\bar{\rho} K_W^H}{r} \frac{\partial}{\partial r} \left(r \frac{\partial q}{\partial r} \right) - \frac{1}{r} \frac{\partial \bar{\rho} u q r}{\partial r} \right\}_{z=z_\beta} \delta_\beta z. \qquad (16)$$

If $S(z_\beta)$ is positive and if parcel ascent from z_β becomes warmer than its environment over some layer, we will assume that the vertical redistribution of the vapor imported into the column in the layer $\delta_\beta z$ is entirely by cumulus convections and that

$$\delta_\beta E = \Delta t S(z_\beta). \tag{17}$$

The left side of (17) is the $\delta_\beta E$ of equation (1). The humidity change at any level z_i in such a column is then

$$\bar{\rho}_i \Delta t \left(\frac{\partial q}{\partial t}\right)_i = \Delta t \lambda_{i,\beta} \left\{ \frac{\bar{\rho} K_W^H}{r} \frac{\partial}{\partial r}\left(r \frac{\partial q}{\partial r}\right) - \frac{1}{r} \frac{\partial \bar{\rho} u q r}{\partial r} \right\}_i + \bar{\rho}_i \Delta_\beta q_i \tag{18}$$

where

$$\lambda_{i,\beta} = \left\{ \begin{matrix} 0 \text{ if } i=\beta \\ 1 \text{ if } i \neq \beta \end{matrix} \right\} \tag{19}$$

and $\Delta_\beta q_i$ is given by equation (7).

When convection originates from n contiguous layers, the humidity change at any level is given by

$$\bar{\rho}_i \Delta t \left(\frac{\partial q}{\partial t}\right)_i = \Delta t \gamma_{i,n} \left\{ \frac{\bar{\rho} K_W^H}{r} \frac{\partial}{\partial r}\left(r \frac{\partial q}{\partial r}\right) - \frac{1}{r} \frac{\partial \bar{\rho} u q r}{\partial r} \right\}_i + \bar{\rho}_i \Delta q_i, \tag{20}$$

where $\Delta q_i = (\Delta q)_{z_i}$ is given by equation (12), and

$$\gamma_{i,n} = \left\{ \begin{matrix} 0 \text{ if } 1 \leq i \leq n \\ 1 \text{ if } i > n \end{matrix} \right\}. \tag{21}$$

The method used to compute nonconvective condensation is described in the appendix.

4. VERTICAL DIFFUSION OF HORIZONTAL MOMENTUM

Vertical transports of horizontal momentum produced by cumulus scale motions play a significant role in the macroscale dynamics of hurricanes (Gray 1967). While Ooyama (1969) provided an explicit parameterization of this effect, Yamasaki (1968a, 1968b) and Rosenthal (1969a, 1969b) have obtained realistic results from their models without explicit representation of the cumulus transports of momentum. However, as will be shown below, their upstream differencing introduces a computational diffusion that behaves somewhat like momentum diffusion by cumuli.

To see this, consider the advective contribution to the momentum tendency in the presence of cumulus activity:

$$\frac{\partial M^*}{\partial t} = -\mathbf{V}^* \cdot \nabla M^* - w^* \frac{\partial M^*}{\partial z}. \tag{22}$$

Asterisks denote the total motion (sum of the mean and eddy components; means are calculated horizontally over a grid interval). Then,

$$M^* = M + M',$$
$$\mathbf{V}^* = \mathbf{V} + \mathbf{V}',$$
and
$$w^* = w + w' \tag{23}$$

where the primes denote eddy components and M, $\mathbf{V}$, and w are the means. From equation (22) and by use of the continuity equation in the form

$$\frac{\partial \rho_S w^*}{\partial z} + \nabla \cdot \rho_S \mathbf{V}^* = 0, \tag{24}$$

we obtain

$$\rho_S \frac{\partial M^*}{\partial t} = -\nabla \cdot \rho_S \mathbf{V}^* M^* - \frac{\partial \rho_S w^* M^*}{\partial z}. \tag{25}$$

Averaging in the usual way, one obtains

$$\frac{\partial M}{\partial t} = -\mathbf{V} \cdot \nabla M - w \frac{\partial M}{\partial z} - \nabla \cdot \overline{\mathbf{V}' M'} - \frac{1}{\rho_S} \frac{\partial \rho_S \overline{w' M'}}{\partial z}. \tag{26}$$

Assume the eddy motion to be produced solely by cumulus activity. Denote values in cloud by $\hat{(\ )}$ and values in clear air by $\tilde{(\ )}$; assume the clouds to cover a fraction α^2 of a grid module. Mean values, M and w, may then be written as

$$M = \alpha^2 \hat{M} + (1-\alpha^2)\tilde{M}$$
and
$$w = \alpha^2 \hat{w} + (1-\alpha^2)\tilde{w}. \tag{27}$$

The eddy correlation then takes the form

$$\overline{M' w'} = \alpha^2(\hat{M}-M)(\hat{w}-w) + (1-\alpha^2)(\tilde{M}-M)(\tilde{w}-w); \tag{28}$$

and by use of (27) to eliminate values in the clear air,

$$\overline{M' w'} = \alpha^2(\hat{M}-M)(\hat{w}-\tilde{w})(1+\alpha^2). \tag{29}$$

Under realistic conditions, $\alpha^2 << 1$ and $\hat{w} >> w$, so

$$\overline{M' w'} \approx \alpha^2 \hat{w}(\hat{M}-M) \approx w(\hat{M}-M). \tag{30}$$

If the air rising in the cumuli tends to conserve M,

$$\hat{M} = M_0. \tag{31}$$

The last term on the right-hand side of equation (26) may then be written as

$$-\frac{1}{\rho_S} \frac{\partial \rho_S \overline{w' M'}}{\partial z} \approx \frac{1}{\rho_S} \frac{\partial}{\partial z} \left\{ \rho_S(z-z_0)w \frac{\partial M}{\partial z} \right\}$$
$$= \frac{1}{\rho_S} \frac{\partial}{\partial z} \left\{ \rho_S G \frac{\partial M}{\partial z} \right\} \tag{32}$$

where the exchange coefficient G is given by

$$G = (z-z_0)w. \tag{33}$$

When the advection equation

$$\frac{\partial A}{\partial t} = -w \frac{\partial A}{\partial z} \tag{34}$$

is differenced with an upstream space difference and a forward time difference, the solution of the resulting difference equation (Molenkamp 1968) is a second-order

approximation to the solution of the differential equation

$$\frac{\partial A}{\partial t} = -w\frac{\partial A}{\partial z} + F_z\frac{\partial^2 A}{\partial z^2} \qquad (35)$$

where the computational viscosity coefficient (F_z) is given by

$$F_z = \tfrac{1}{2}|w|\Delta z\left\{1 - \frac{|w|\Delta t}{\Delta z}\right\} \equiv k^2|w|\Delta z. \qquad (36)$$

While the general similarity of expressions (33) and (35) is clear, there are some important differences. The most significant of these is that the former appears in (32) as a conservation form and, therefore, makes no contribution to the vertically integrated value of M. The computational diffusion will, however, effect the vertically integrated value of the quantity A (equation 35). Despite this, section 9 will show that velocity distributions obtained from numerical experiments with upstream differencing of vertical advection terms are far more realistic than those obtained with centered differencing. These results clearly indicate that the computational diffusion, in some sense, tends to simulate the momentum transports by cumulus.

5. REVIEW OF THE MODEL

The model uses the primitive equations, assumes circular symmetry, and has seven levels (table 1). The system is open at the lateral boundary. The basic equations are

$$\frac{\partial M}{\partial t} = -u\frac{\partial M}{\partial r} - w\frac{\partial M}{\partial z} - fru + \frac{1}{\bar{\rho}}\frac{\partial}{\partial z}\left(\bar{\rho}K_M^z\frac{\partial M}{\partial z}\right)$$
$$+ \frac{K_M^H}{r}\frac{\partial}{\partial r}\left\{r^3\frac{\partial}{\partial r}\left(\frac{v}{r}\right)\right\}, \qquad (37)$$

$$\frac{\partial u}{\partial t} = -u\frac{\partial u}{\partial r} - w\frac{\partial u}{\partial z} + \frac{M}{r}\left(f + \frac{M}{r^2}\right) - \theta\frac{\partial \phi}{\partial r}$$
$$+ \frac{1}{\bar{\rho}}\frac{\partial}{\partial z}\left(\bar{\rho}K_M^z\frac{\partial u}{\partial z}\right) + \frac{K_M^H}{r^2}\frac{\partial}{\partial r}\left\{r^3\frac{\partial}{\partial r}\left(\frac{u}{r}\right)\right\}, \qquad (38)$$

$$\frac{\partial \theta}{\partial t} = -u\frac{\partial \theta}{\partial r} - w\frac{\partial \theta}{\partial z} + \frac{c_p K_T^H}{r\phi}\frac{\partial}{\partial r}\left(r\frac{\partial \theta}{\partial r}\right) + \frac{\dot{Q}}{\phi}, \qquad (39)$$

$$\frac{\partial \phi}{\partial z} = -\frac{g}{\theta}, \qquad (40)$$

$$\frac{\partial \bar{\rho}w}{\partial z} = -\frac{1}{r}\frac{\partial \bar{\rho}ru}{\partial r}, \qquad (41)$$

$$\phi = c_p(p/p_0)^{R/c_p}, \qquad (42)$$

$$\theta\phi = c_p T, \text{ and} \qquad (43)$$

$$M = rv. \qquad (44)$$

Equations (37) and (38) are forms of the tangential and radial equations of motion, respectively. Equation (39) is the thermodynamic equation. Equation (40) is the hydrostatic equation and (41) is a form of the continuity equation that is easily justified by an order of magnitude

analysis and has been used by others (Charney and Eliassen 1964) for the hurricane problem.

Boundary conditions on the vertical motion at the top and bottom levels are

$$w_1 = w_7 = 0 \qquad (45)$$

where the subscript denotes level.

Equations (41) and (45) filter the external gravity wave and thus allow larger time steps. However, as shown below, they place a restriction on the pressure field that must be retained in the numerical model for physical consistency. From (41) and (45),

$$\int_{z_1}^{z_7} \bar{\rho}u\,dz = 0. \qquad (46)$$

From (38) and (46),

$$\int_{z_1}^{z_7}\bar{\rho}\theta\frac{\partial\phi}{\partial r}dz = \int_{z_1}^{z_7}\bar{\rho}\left\{\frac{M}{r}\left(f + \frac{M}{r^2}\right) - u\frac{\partial u}{\partial r} - w\frac{\partial u}{\partial r}\right\}dz$$
$$+ \int_{z_1}^{z_7}\bar{\rho}\left\{\frac{K_M^H}{r^2}\frac{\partial}{\partial r}\left[r^3\frac{\partial}{\partial r}\left(\frac{u}{r}\right)\right]\right.$$
$$\left. + \frac{1}{\bar{\rho}}\frac{\partial}{\partial z}\left(\bar{\rho}K_M^z\frac{\partial u}{\partial z}\right)\right\}dz \equiv B. \qquad (47)$$

By use of the hydrostatic equation (40),

$$\int_{z_1}^{z_7}\bar{\rho}\theta\frac{\partial\phi}{\partial r}dz = \frac{\partial\phi_1}{\partial r}\int_{z_1}^{z_7}\bar{\rho}\theta dz - \int_{z_1}^{z_7}\bar{\rho}\theta\frac{\partial H}{\partial r}dz \qquad (48)$$

in which

$$H = \int_{z_1}^{z}\frac{g}{\theta}dz' \qquad (49)$$

where z' is a dummy variable. From (47), (48), and (49),

$$\frac{\partial\phi_1}{\partial r} = \frac{B + \int_{z_1}^{z_7}\bar{\rho}\theta\frac{\partial H}{\partial r}dz}{\int_{z_1}^{z_7}\bar{\rho}\theta dz}. \qquad (50)$$

The manner in which the restriction (50) is employed in the computational cycle is shown in the appendix.

Discarding viscous and diabatic effects, the system of equations with the boundary condition (45) gives the energy integral

$$\frac{\partial}{\partial t}\int_0^{z_7}\int_0^{r^*}\bar{\rho}\left\{\frac{u^2 + v^2}{2} + c_p T + gz\right\}r\,dr\,dz$$
$$= \int_0^{z_7}\int_0^{r^*}\left(\frac{\bar{\rho}}{\rho}\right)\frac{\partial p}{\partial t}r\,dr\,dz, \qquad (51)$$

provided that the domain is mechanically closed at $r = r^*$. If the complete form of the continuity equation

$$\frac{\partial\rho}{\partial t} = -\frac{\partial\rho w}{\partial z} - \frac{1}{r}\frac{\partial\rho ru}{\partial r}$$

is used in place of (41), the energy integral analogous to

TABLE 1.—*Heights and mean pressures of the information levels. The mean pressures are approximate and are based on a mean hurricane season sounding (Hebert and Jordan 1959).*

Level	Height	Mean pressure
	(meters)	*(millibars)*
1	0	1015
2	1054	900
3	3187	700
4	5898	500
5	9697	300
6	12423	200
7	16621	100

(51) is

$$\frac{\partial}{\partial t}\int_0^{z_1}\int_0^{r^*} \rho\left(\frac{u^2+v^2}{2}+c_pT+gz\right)rdrdz=\int_0^{z_1}\int_0^{r^*}r\frac{\partial p}{\partial t}drdz \tag{52}$$

that can be written in the more familiar form

$$\frac{\partial}{\partial t}\int_0^{z_1}\int_0^{r^*} \rho\left(\frac{u^2+v^2}{2}+c_vT+gz\right)rdrdz=0. \tag{53}$$

By comparison of (51) and (52), we see that the model is only approximate in its conservation of total energy.

Time derivatives are estimated by forward differences except in the case of specific humidity where a Matsuno (1966) type integration is employed. Advective derivatives are calculated by the upstream method except for the special experiments described in section 9 and for the case of humidity where a conservation form of the equations is used. All nonadvective space derivatives are calculated as centered differences. All variables are defined at all levels. Vertical integrals are evaluated by trapezoidal integration.

Grid points in the radial direction are staggered. Horizontal velocity is defined at the radii

$$r_j=(j-1)\Delta r, \quad j=1, 2, \ldots. \tag{54}$$

Temperature, pressure, vertical motion, and humidity are carried at the radii

$$r_j=(j-\tfrac{1}{2})\Delta r, \quad j=1, 2, \ldots. \tag{55}$$

Air-sea exchanges of sensible and latent heat are simulated by the pragmatic constraint that relative humidity and temperature are invariant in both space and time at levels 1 and 2. On the other hand, the surface stresses in the equations of motion are treated explicitly by use of a drag coefficient and the usual quadratic stress law. That is, to evaluate vertical mixing terms at levels 1 and 2, we invoke the boundary conditions

$$\left(\bar\rho K_M^z\frac{\partial M}{\partial z}\right)_{z_1}=C_D\bar\rho_1|\mathbf{V}|_1 M_1 \tag{56}$$

and

$$\left(\bar\rho K_M^z\frac{\partial u}{\partial z}\right)_{z_1}=C_D\bar\rho_1|\mathbf{V}|_1 u_1 \tag{57}$$

where C_D is the (constant) drag coefficient and

$$|\mathbf{V}_1|=(u_1^2+v_1^2)^{1/2}.$$

Equations (37) and (38) are applied at the radial grid given by (54) and at vertical grid points $i=1,2, \ldots, 7$. At $j=1$ (where $r=0$),

$$M=0 \text{ and } u=0. \tag{58}$$

At $j=J_{max}$ (where $r= 440$ km),

$$(ru)_{J_{max}}=(ru)_{J_{max}-1} \tag{59}$$

and

$$M_{J_{max}}=M_{J_{max}-1} \tag{60}$$

which are the conditions, respectively, that the horizontal divergence and relative vorticity vanish.

The potential temperature tendencies are evaluated on the radial grid defined by equation (55) and at the vertical grid points $i=3, \ldots, 7$. At $i=1$, 2, the potential temperatures are computed from (43) so that the temperature is maintained at its initial value. The boundary condition at J_{max} for potential temperature is

$$\theta_{J_{max}}=\theta_{J_{max}-1}. \tag{61}$$

An outline of the complete computational cycle is found in the appendix.

6. EXPERIMENT W1

The results of experiment W1 are fairly typical of what can be expected of the model. A number of parameters utilized in experiment W1 are listed in table 2. For computational economy, the first 72 hr of the calculation were conducted with 20-km radial resolution and a time step of 120 sec. The data were then linearly interpolated to a 10-km grid, and the calculation was continued on the finer mesh with a time step of 60 sec. Friction and viscosity coefficients were established largely by trial and error.

The initial conditions of wind, pressure, and temperature are identical to those used in our previous experiments and consist of a weak vortex in gradient balance with zero meridional circulation. The central pressure is 1013 mb; the maximum wind is 7 m sec^{-1} and is located at a radius of approximately 250 km. The mathematical derivation of this balanced state is also given in the appendix.

The initial field of specific humidity varies only with height and corresponds approximately to relative humidities (table 3) that are very nearly equal to those of the mean tropical atmosphere (Hebert and Jordan 1959). As before, the mathematical details of the initialization are given in the appendix.

Figure 2 summarizes the storm's evolution at sea level. The "organizational" period consisting of the first three or so days is characteristic of tropical cyclone models that are initialized with nondivergent winds (Ooyama 1969, Rosenthal 1969a and 1969b) and seems to have a counterpart in nature (see section 8). The intensification that occurs between 72 and 96 hr is not related to the change in radial resolution introduced at hour 72 since, as will be shown in the next section, nearly the same intensification takes place if the mesh is not refined.

The storm reaches peak intensity at about hour 144. The central pressure and strongest surface wind at this time are 976 mb and 45 m sec^{-1}, respectively. Hurricane-force winds are present from about 108 hr to the end of the calculation. The radius of maximum surface wind decreases rapidly during the deepening period and is more or less constant therafter.

Figures 3, 4, 5, 6, and 7 illustrate various aspects of the storm structure and confirm that the model yields results that are quite reasonable. While it is not shown on figure 7, the vertical motion pattern contains a narrow zone of upper tropospheric subsidence at the storm center. The old model showed a more distinct "eye" (Rosenthal 1969b).

Average rainfall rates for the inner 100 km of the storm circulation are shown by figure 8. From 96 to 216 hr, the total rainfall averages about 25 cm day^{-1} or, roughly, 10 in. per day, a quite reasonable rate. The nonconvective rainfall is about two-thirds of the convective precipitation. According to Hawkins and Rubsam (1968), radar data gathered in hurricane Hilda (1964) indicate substantial rain from stratiform clouds. Their observations also indicate that, while a large portion of Hilda's circulation contained appreciable rain, active cumulonimbi were present only in the eye wall region. In view of these observations, the partitioning of rain between convective and nonconvective components (fig. 8) is acceptable.

Figure 8 also illustrates the efficiency of the inner 200 km of the storm. This quantity is defined in the usual manner (Palmén and Riehl 1957) as the ratio of the rate of kinetic energy production to the rate of latent heat release. The values during the mature stage are quite close to the empirical value of 2.7 percent found by Palmén and Riehl (1957).

The generation of available potential energy[2] (fig. 9) during the mature stage is fairly close to the empirical estimate made by Anthes and Johnson (1968) for hurricane Hilda (1964). Figure 9 also shows that nonconvective condensation provides a substantial part of the generation and that virtually all of the generation occurs in the inner 100 km.

The kinetic energy content of various rings of the model storm are shown by figure 10. In comparison to the old model (Rosenthal 1969a, 1969b), there is a dramatic improvement in the behavior of the outer rings of the storm. In the 300–400-km ring, the old model showed a monotonic increase of kinetic energy with time. Figure 10, on the other hand, shows that this is not the case with the new model where a definite maximum of kinetic energy is reached before the calculation is terminated.

Figure 11 shows the kinetic energy budget as a function of time (the details of the computation are described in the appendix). The contributing terms, in a relative sense, behave in a fashion similar to that found for the old model (Rosenthal 1969a, 1969b). However for the storm as a whole (0–400-km radial interval), the magnitudes of the

[2] The computational equations are given in the appendix.

TABLE 2.—*Parameters for experiment* W1

Parameter	Symbol	Value
Time increment	Δt	60 sec
Radial increment	Δr	10 km
Radial limit of computational domain		440 km
Kinematic coefficient of eddy viscosity for lateral mixing of momentum	K_M^H	10^3 m^2 sec^{-1}
Kinematic coefficient of eddy conductivity for lateral mixing of heat	K_T^H	10^4 m^2 sec^{-1}
Kinematic coefficient of eddy conductivity for lateral mixing of water vapor	K_W^H	10^4 m^2 sec^{-1}
Drag coefficient	C_D	3×10^{-3}
Kinematic coefficient of eddy viscosity for vertical mixing of momentum	K_M^z	10 m^2 sec^{-1} at level 1, 5 m^2 sec^{-1} at level 2, 0 elsewhere

TABLE 3.—*Initial values of relative humidity at the information levels*

Level	Height	Relative humidity
	(*meters*)	(*percent*)
1	0	90
2	1054	90
3	3187	54
4	5898	44
5	9697	30
6	12423	30
7	16621	30

---

various terms are about half that found with the old model. The difference is largely due to the fact that the outer rings of the new model are far more inert energetically than is the case for the old model.

Loss of energy through truncation errors (computed as a residual in the budget equation, see appendix) is comparable in magnitude to the surface dissipation by drag friction. The major portion of this truncation error can be accounted for by computational diffusion in the sense of Molenkamp (1968).

Figures 12 and 13 illustrate the computational (or, in Molenkamp's terminology, the "pseudo") viscosity coefficients calculated for experiment W1. In the mature stage, the coefficient for lateral mixing averaged over the entire storm is about 5×10^3 m^2 sec^{-1}. This is five times greater than the explicit coefficient for momentum (table 2). In the inner 100 km, the computational coefficient for lateral mixing averages over 10^4 m^2 sec^{-1}, while for vertical mixing this coefficient is about an order of magnitude greater than its average value for the storm as a whole.

Figures 14 compares the explicit dissipation of kinetic energy with the total (explicit plus computational). Details of the calculation are presented in the appendix. The figure shows the unexplained truncation error to be fairly small. Despite the extremely large coefficients for vertical computational diffusion, the kinetic energy dissipation due to this effect is quite small compared to dissipation by drag friction at the lower boundary. The bulk of the truncation error is produced by upstream differencing of horizontal advection terms. This will be discussed in greater detail in section 9.
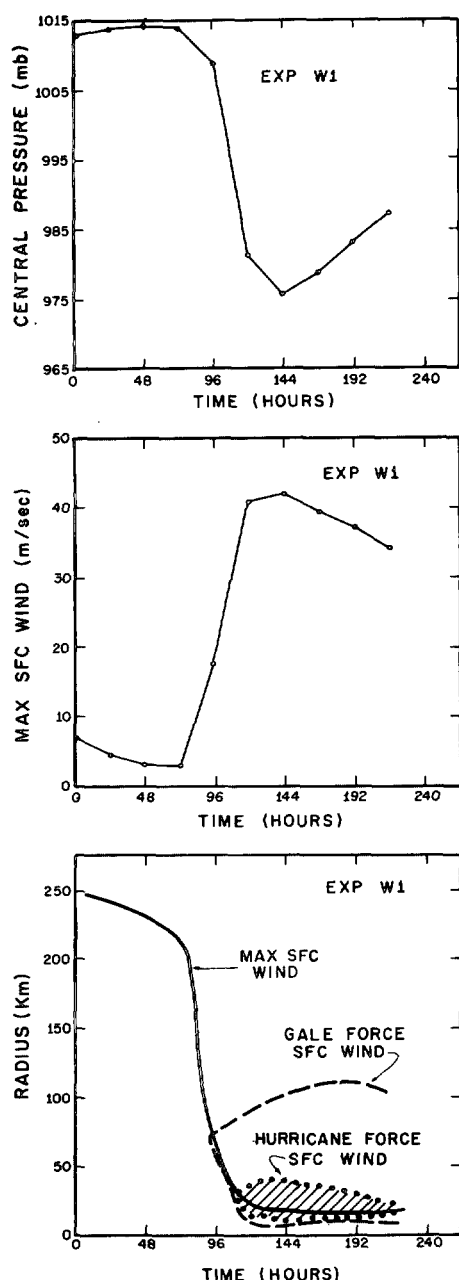
FIGURE 2.—Results from experiment W1. Top, central pressure as a function of time; center, maximum surface wind as a function of time; bottom, radii of maximum surface wind and inner and outer limits of hurricane-force and gale-force winds at the surface.

FIGURE 3.—Results from experiment W1, radial profiles of surface wind speed.

7. EXPERIMENT W2

As noted in section 1, the experiments discussed in later sections of this report were conducted with 20-km radial resolution. Because of this, we present a brief summary of experiment W2 that is identical to W1 in all respects except for the values of Δr and Δt; these are 20 km and 120 sec, respectively. The first 72 hr are, of course, identical to those of W1.

Central pressures [3] and maximum surface winds for the two experiments are compared in the upper two graphs

in figure 15. After hour 72, W1 deepens somewhat more rapidly at first; but in both experiments, greatest intensity is reached by about hour 144. At this time, W1 is 8 mb deeper in central pressure, and maximum surface winds differ by about 4 m sec^{-1}.

After hour 144, experiment W1 decays more rapidly; and when the two calculations are terminated at hour 216, central pressures and maximum surface winds are very nearly the same.

By comparison of the bottom sections of figures 2 and 15, we find that W2 develops a somewhat larger storm, as was to be expected. Differences are, however, much less than was the case when the resolution was varied in the old model.

The surface pressure and wind profiles for experiment W2 (not shown) are similar to those obtained from W1
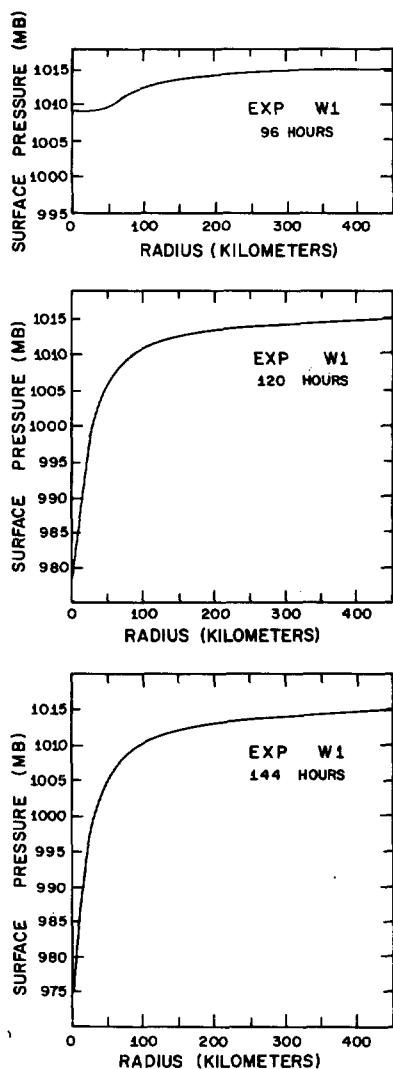
---

[3] Pressure is not defined at zero radius because of the grid staggering (equations 54 and 55). Central pressure values presented in this paper are, therefore, pressure values at $z=0, r=\Delta r/2$.

FIGURE 4.—Results from experiment W1, radial profiles of surface
pressure.

FIGURE 5.—Results from experiment W1, radial profiles of vertical
velocity at the 1054-m level.

(figs. 3 and 4). The profiles of vertical motion at level 2
(not shown) indicate boundary layer convergence to be
30 to 50 percent weaker than that for W1, but to cover a
broader horizontal area. Experiment W2, therefore, gives
a broader but weaker convection zone. Vertical cross
sections of the dependent variables at hour 144 of
experiment W2 (not shown) are similar to those for W1
(figs. 6 and 7).

Rainfall rates and efficiencies for W2 (fig. 16) except
for the sharp peaks near hour 108 are just slightly larger
than those of W1 (fig. 8). The kinetic energy content of
the inner 100 km of W2 (not shown) is very nearly the
same as for W1 (fig. 10). In the outer rings of the storm,
however, W2 contains somewhat more kinetic energy.

Overall, it seems fair to conclude that results with
20-km radial resolution are fairly representative of those
obtained with 10-km resolution. The larger radial incre-
ment leads to a larger storm with greater kinetic energy
in the outer portions of the circulation. The differences
are, however, relatively minor and far less than those
found with the old model.

8. EFFECTS OF THE INITIAL HUMIDITY DISTRIBUTION

Riehl (1954) emphasizes that tropical storms form only
in preexisting disturbances and that deepening is usually
a slow process which requires several days. This "organi-
zational" period is evident in the experiments described
above. As also noted by Riehl (1954), large moisture
content to great heights seems to be necessary before
substantial deepening will occur. In the early stages of
development when low-level convergence is still relatively
weak, a deep moist layer would seem essential if entraining
cumulus with small horizontal cross sections are to grow
in the vertical and reach the cumulonimbus stage.

On the other hand, the depth of the moist layer is tuned
to the macroscale motion (Riehl 1954) and increases with
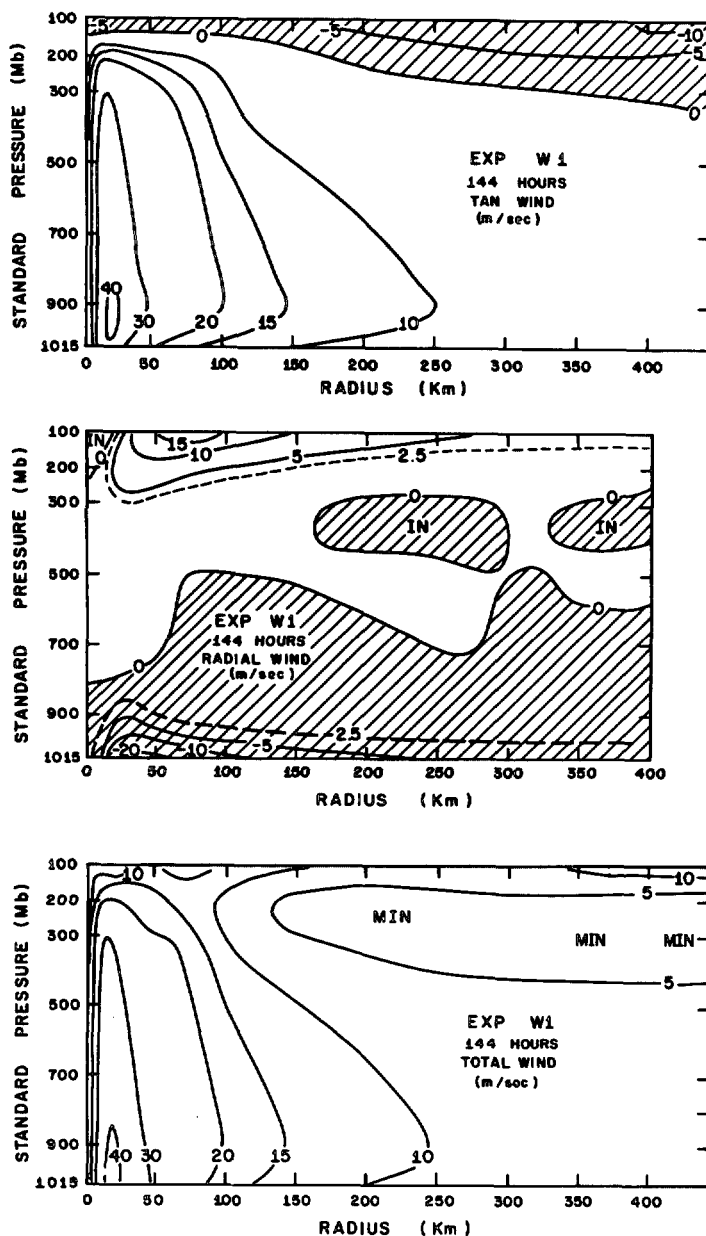low-level convergence. The role of the preexisting dis-

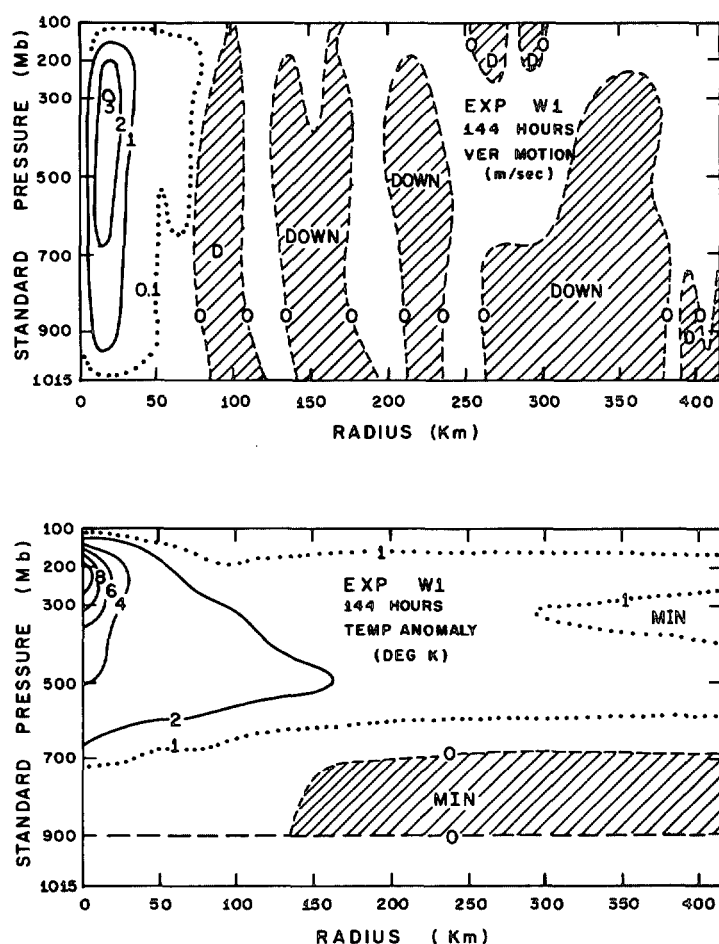FIGURE 6.—Results from experiment W1 at hour 144. Top, cross section of tangential wind; center, radial wind; bottom, total wind.

FIGURE 7.—Results from experiment W1 at hour 144. Top, cross section of vertical motion; bottom, temperature anomaly.

turbance or "organizational period" may well be the development of the required deep moist layer from a humidity distribution that initially approximates that of the mean tropical atmosphere. Once the moist layer had been developed, cumulus cells entrain relatively moist air, making their growth to the cumulonimbus stage more likely. With the onset of increased cumulonimbus activity, the chances of rapid development of the macroscale disturbance would seem to be better than before.

While the convective adjustment described in section 2 does not contain an explicit representation of entrainment (and, indeed, assumes the cumulus to rise with undilute ascent), the sense of the sequence described above is simulated. The partitioning of condensate between precipitation and reevaporation depends directly on the

difference between cloud and environmental humidities (equations 4, 7, and 8). Hence, a model atmosphere that is drier will have substantially less precipitation and, hence, less macroscale heating. On this basis, it seems reasonable to argue that a shorter organizational period would be present if the initial humidity were greater.

Experiment W6, which differs from W2 only in that the initial relative humidity is 90 percent everywhere, tests this hypothesis. Central pressures and maximum surface winds obtained from the two experiments (fig. 17) seem to verify the arguments of the previous paragraph. While the peak surface winds and deepest central pressures are about the same for the two calculations, those for W6 occur about 48 hr earlier than those for W2. An organizational period of 72 hr is required for development in W2, but only 24 hr is needed in W6. From figures 16 and 18, we find the average rainfall for W6 to be about 10 cm per day greater than that for W2. Maximum efficiencies for the two experiments are very nearly the same.

9. FURTHER CONSEQUENCES OF UPSTREAM DIFFERENCING

In section 6, it was shown that the truncation errors due to upstream differencing play an important role in the kinetic energy budget of the model storm. Further-
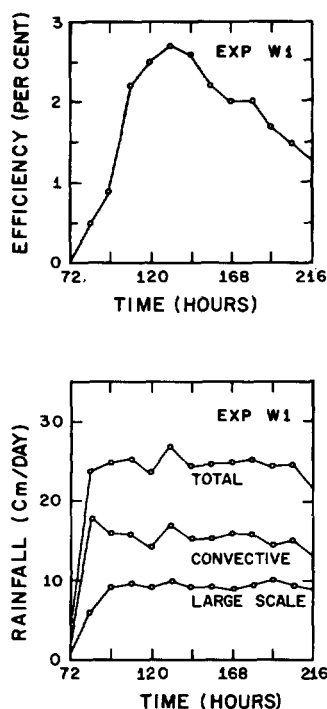
FIGURE 8.—Results from experiment W1. Top, efficiency of the radial interval 0 to 200 km; bottom, average rainfall over the radial interval 0 to 100 km.

more, we found that the bulk of the total internal dissipation of kinetic energy (explicit lateral mixing plus computational lateral and vertical mixing) is produced by upstream differencing of the horizontal advection terms.

It has been our stated intention (Rosenthal 1969a) to reformulate the model in a more accurate difference scheme at a time when this became economically feasible. In this section, we will show the results of a number of experiments (table 4) in which various advection terms in the equations of motion and in the thermodynamic equation were estimated by a centered finite-difference analog. (The water vapor equation, however, was not altered and, hence, is treated as described earlier.) The numerical technique ,adopted for this purpose is the second-order advection form given by Crowley (1968). This method employs forward time steps and, therefore, required minimal modification of the original program.

To calculate vertical advection, Crowley's equations were modified to take into account the variable vertical resolution (table 1) employed in our model. This modification was made in such a way that the second-order accuracy of the technique was preserved. For linear advection with a constant advecting velocity, Crowley's scheme reduces to the Lax-Wendroff method. It is, therefore, a damping system but far less so than the upstream method (Crowley 1968).

Parameters not listed in table 4 are identical to those used for experiment W2. Initial conditions are again hour 72 of experiment W2.

In experiment WC1, the explicit parameters are identical to those of experiment W2. The two experiments differ
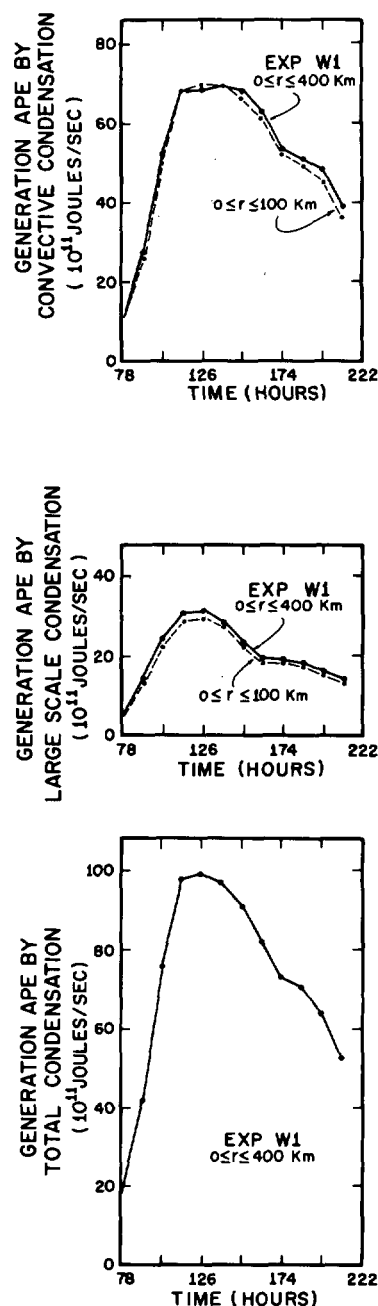

FIGURE 9.—Results from experiment W1. Top, generation of available potential energy by convective condensation heating; solid line is for radial interval 0 to 400 km; dashed line is for radial interval 0 to 100 km; center, generation of available potential energy by large-scale condensation heating; bottom, generation of available potential energy by total condensation heating.

only in the finite-difference analogs to the advection terms in the equations of motion and in the thermodynamic equation. In view of the crucial role played by computational diffusion in experiment W2, it was anticipated that this experiment would give unrealistic results; it was necessary to terminate the calculation after 17 hr because limits on the table used to compute temperatures along the pseudoadiabats had been exceeded. Tangential winds in excess of 100 m sec^{-1} and radial winds over 50 m sec^{-1} had already been generated. The structure was completely unrealistic, showing large amplitude waves in the radial
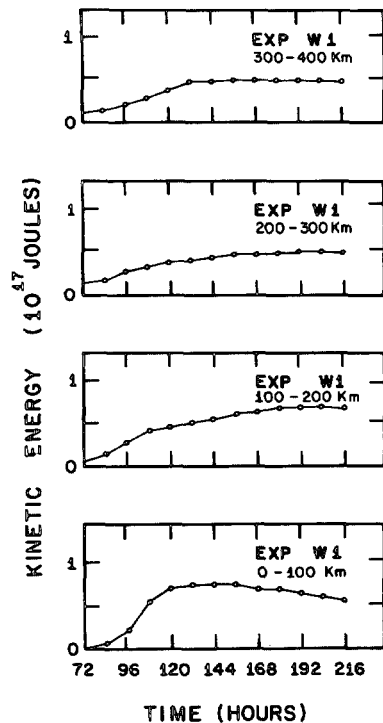
FIGURE 10.—Results from experiment W1, variation with time of the kinetic energy content of various rings of the storm.
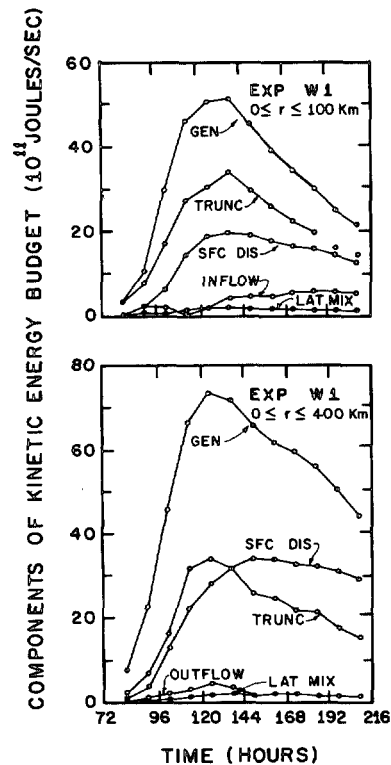
FIGURE 11.—Results from experiment W1, components of the kinetic energy budget as a function of time. "GEN" is generation; "TRUNC" is dissipation by truncation error computed as a residual in the budget equation; "SFC DIS" is dissipation by drag friction at the surface; "LAT MIX" is dissipation by explicit lateral mixing. Top, radial interval 0 to 100 km; bottom, radial interval 0 to 400 km.
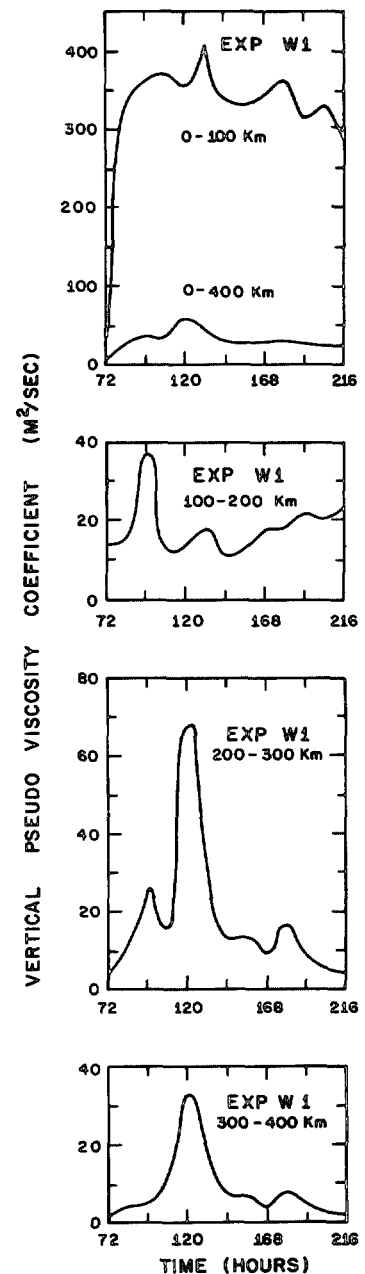
FIGURE 12.—Results from experiment W1, variation with time of the mass-averaged computational, or pseudo, coefficient of vertical viscosity for various radial intervals. The scale of the top graph differs from that of the others.

direction. It was clear that the explicit lateral mixing coefficients (table 4) were too small.

The computational viscosity coefficients for experiment W2 (figure not shown) were used as a basis for selecting a value of 2×10^4 m^2 sec^{-1} for the diffusion coefficients for heat, momentum, and water vapor to be used in experiment WC2. All other aspects of WC2 are identical to those for WC1.

Experiment WC2 was terminated after hour 24. Surface winds over 58 m sec^{-1} had already been generated. While the radial profiles of wind and pressure in the boundary
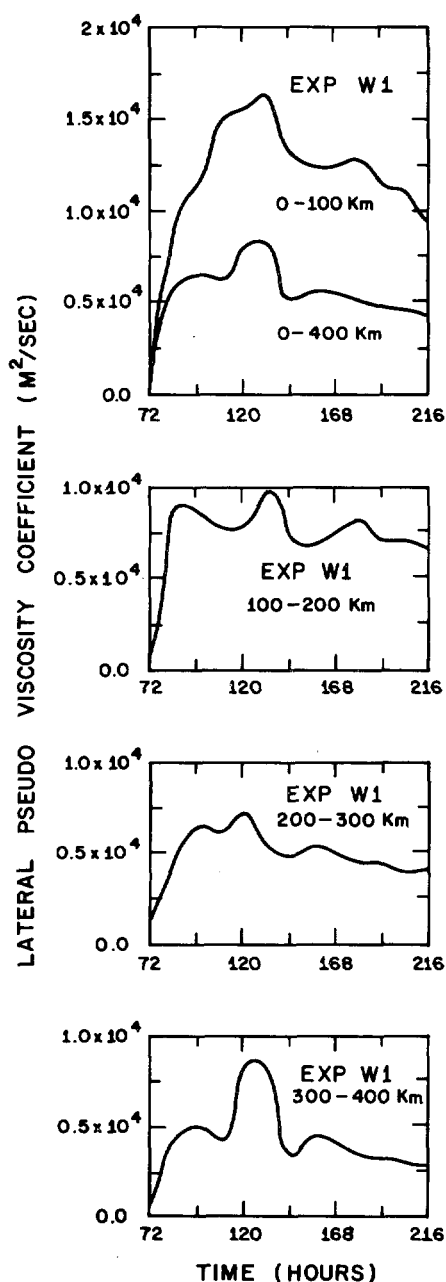
FIGURE 13.—Results from experiment W1, same as figure 12 but for lateral viscosity.
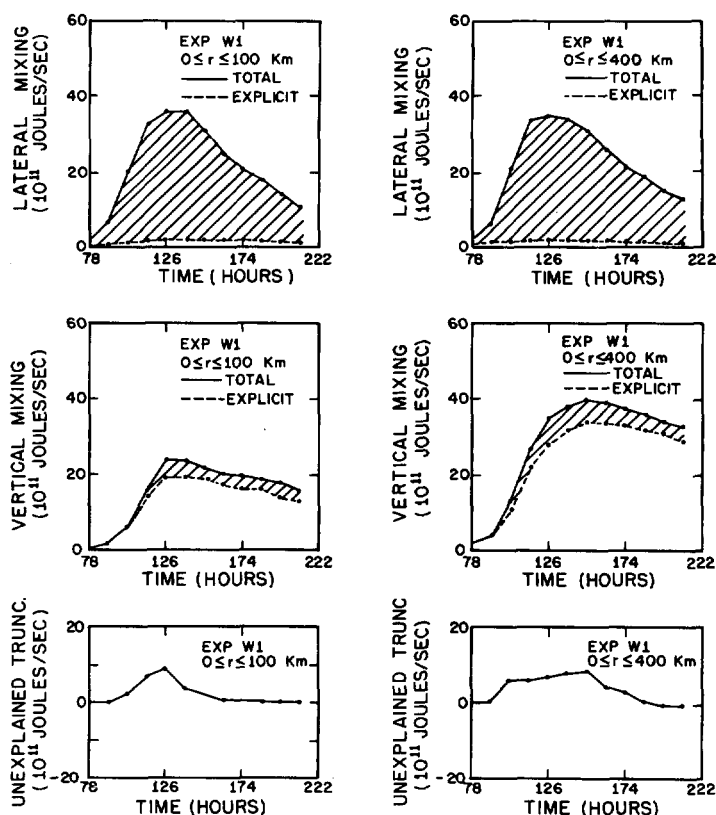

FIGURE 14.—Results from experiment W1. Top, explicit dissipation of kinetic energy by lateral viscosity (dashed) and total lateral dissipation by the sum of explicit and computational lateral viscosity (solid) for radial intervals of 0–100 km and 0–400 km; center, dissipation of kinetic energy by surface drag friction (dashed) and total of dissipations by surface drag and computational vertical viscosity for radial intervals of 0–100 km and 0–400 km; bottom, truncation error that remains in the kinetic energy budget after the truncation error due to upstream differencing is subtracted.

layer were fairly realistic, there were serious deficiencies in the vertical structure. These are illustrated by a cross section of tangential wind (fig. 19). The outward slope of the wind maximum and the strong vertical gradients of wind in the inner 50 km are entirely unrealistic and far different from the pattern obtained in experiment W2 (similar to fig. 6).

This deficiency of WC2 is clearly related to the lack of a parametric representation of vertical transport of horizontal momentum by cumulus and other subgrid eddies. In experiments W1 and W2, the upstream differencing of the vertical advection terms (section 4) tends

to compensate for the lack of an explicit representation of the cumulus diffusion.

Experiment WC3 differs from WC2 only in the differencing of the vertical advection terms in the equations of motion. For including some sort of analog to the momentum diffusion by cumulus, upstream differencing is used for $w(\partial M/\partial z)$ and $w(\partial u/\partial z)$. Crowley's scheme is retained for all horizontal advections and also for $w(\partial\theta/\partial z)$ since the convective adjustments described in section 2 are intended to simulate the total effect on the macroscale of the cumulus (vertical heat transport as well as condensation).

As measured by central pressure and surface wind, experiment WC3 reached peak intensity at hour 96 (or just 24 hr after its start) with surface winds of 44 m sec^{-1}. The tangential wind pattern at this time is shown by figure 20. In comparison to experiment WC2 (fig. 19), the pattern is much more realistic. However, the overall results from WC3 are far from satisfactory, as can be
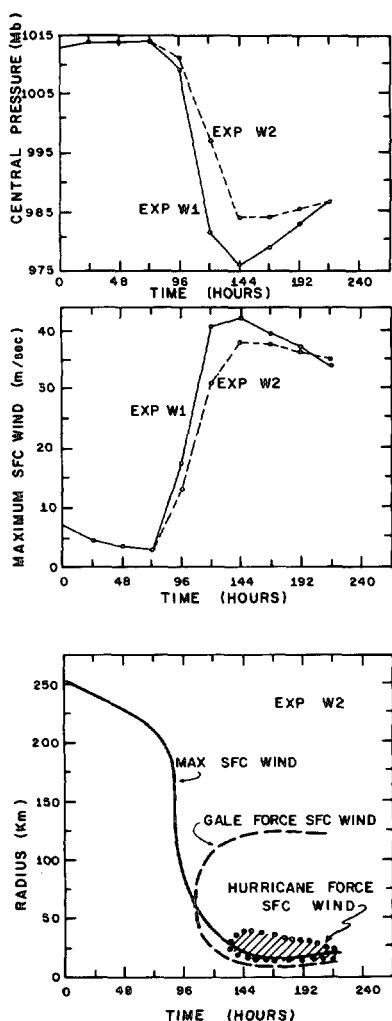
FIGURE 15.—Top, comparison of central pressure as a function of time for experiments W1 and W2; center, comparison of maximum surface winds for experiments W1 and W2; bottom, results from experiment W2. Radii of maximum surface wind and inner and outer limits of hurricane-force and gale-force winds at the surface.
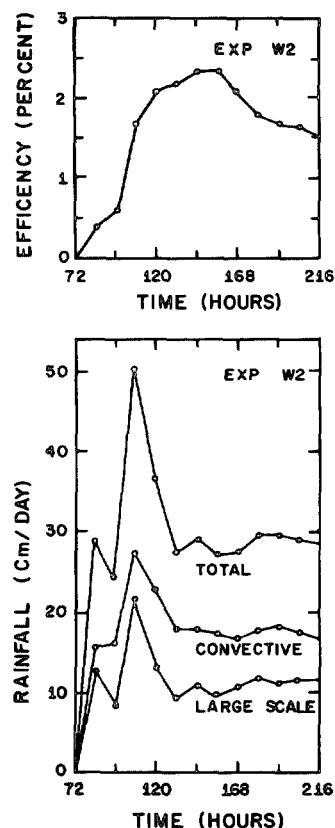

FIGURE 16.—Results from experiment W2. Top, efficiency of the radial interval 0 to 200 km; bottom, average rainfall over the radial interval 0 to 100 km.

verified from figure 21; this figure shows that the storm expends at an unreasonable rate during its decay.

Clues to the explanation of this rapid expansion are found in the sequence of temperature patterns shown by figure 22. In all previous experiments, largest temperature anomalies at the storm center have always been at the 200-mb level, in agreement with observations. In contrast, figure 22 shows experiment WC3 to produce its largest temperature anomaly at 300 mb. A second point of importance lies in the rapid destruction of the horizontal temperature gradient. We will see below that both of these difficulties appear to be produced by truncation errors in the calculation of $w(\partial\theta/\partial z)$ and, surprisingly enough, the upstream method provides a more accurate result.

The full curve on figure 23 shows the base state potential temperature plotted from the data given by table 2. This is the thermal structure that the model "sees." The dashed curve shows the thermal structure obtained when all data points given by Hebert and Jordan (1959) are plotted. The slope of the solid curve between 200 and 100 mb is

substantially greater than the actual slope at 200 mb (if the dashed curve is taken as the standard). On this basis, we might anticipate that a noncentered difference using 200- and 300-mb data might provide a better estimate of $w(\partial\theta/\partial z)$ at 200 mb than would a centered technique using 300-, 200-, and 100-mb data.

If we assume an upward vertical velocity of 1 m sec⁻¹ and take a time step of 120 sec, the contribution to the potential temperature change at 200 mb due to vertical advection based on the dashed curve and using Crowley's second-order advection form is −0.439°K. If we take this as a "true" value and apply the same technique to the solid curve using the 100-, 200-, and 300-mb data, we obtain −0.682°, a 55 percent overestimate of the adiabatic cooling. The upstream method gives −0.310° which is a 29 percent underestimate of the cooling.

Therefore, with the resolution of the seven-level model and with the thermal structure of the mean tropical atmosphere, the second-order advection form overestimates adiabatic cooling at the 200-mb level. The upstream method underestimates this effect but comes closer to that which would be obtained if the model had greater vertical resolution.

This type of truncation error in WC3 accounts for both the displacement of the maximum temperature anomaly to 300 mb and for the rapid destruction of the temperature gradient since the convective heat supply is simply unable to sufficiently compensate for the excessive adiabatic cooling at 200 mb.
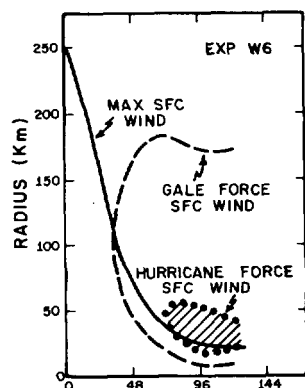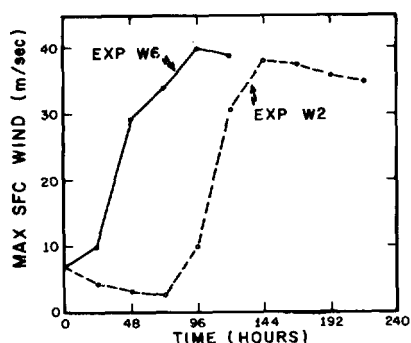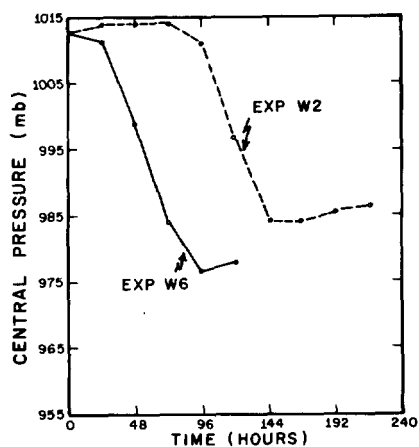
FIGURE 17.—Top, comparison of central pressure as a function of time for experiments W2 and W6; center, comparison of maximum surface wind for experiments W2 and W6; bottom, results from experiment W6. Radii of maximum surface wind and inner and outer limits of hurricane-force and gale-force winds at the surface.
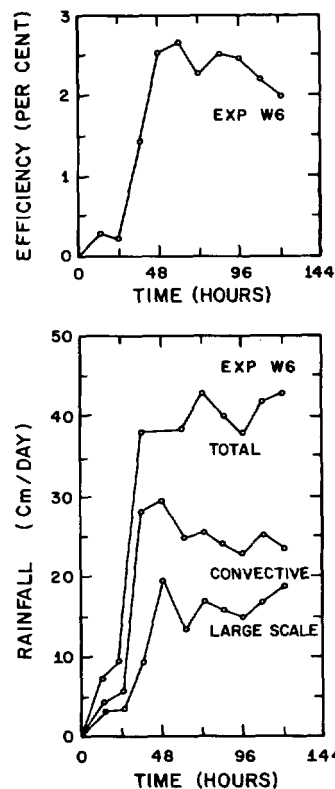

FIGURE 18.—Results from experiment W6. Top, efficiency of the radial interval 0 to 200 km; bottom, average rainfall over the radial interval 0 to 100 km.

Experiment WC4 differs from WC3 only in its use of the upstream method for calculation of $w(\partial\theta/\partial z)$. A sequence of temperature patterns obtained from WC4 is shown by figure 24. Despite some obviously unrealistic features in the lower troposphere, the arguments of the previous paragraph appear to be verified; the greatest temperature anomaly is at 200 mb, and the upper tropospheric temperature gradient remains concentrated near the storm center. The lower section of figure 25 shows that WC4 does not expand without limit as was the case for WC3.

Further information on the structure of WC4 is given by figure 26. While the results obtained from WC4 are more realistic than those obtained from WC3, they are clearly inferior to those of experiments W1 and W2.

This is also indicated by the upper section of figure 25 that shows the central pressures obtained from WC4 to be too high to be empirically consistent with the wind speeds. This is verified by figure 27 based on the work of Colón (1963). Colón presents a scatter diagram of central pressure versus maximum wind based on a number of tropical storm and hurricane observations in various stages of the life cycle (genesis, maturity, dissipation). The two straight lines on figure 27 are drawn to contain almost all of Colón's data points. Also plotted on the diagram are the data points obtained from WC4. At hours 120 and 144, the WC4 points fall outside the envelope and indicate winds to be too strong for the central pressure. While two of Colón's points also fall outside these lines, a reduction of only 2 kt in wind would bring them into the envelope. On the other hand, the WC4 wind at hour 144 would have to be reduced by about 12 kt to obtain agreement. The data points for W2 (fig. 28) all fall well within the limits of Colón's data.

The deterioration of the solutions with the introduction of the centered difference scheme was not anticipated and, indeed, was quite disappointing. Not only does the less accurate upstream method provide model storms with more acceptable structure and better consistency between wind and pressure but also consistency provides an internal dissipation of kinetic energy of the same order of magnitude as the surface dissipation (section 6 and Rosenthal 1969a, 1969b). It appears (Miller 1962, Riehl and Malkus 1961) that this is the correct proportionality between in-

TABLE 4.—*Summary of experiments that vary finite-difference analogs to advective terms*

Experiment no.	K_W^H (m² sec⁻¹)	K_M^H (m² sec⁻¹)	K_T^H (m² sec⁻¹)	$w(\partial\theta/\partial z)$	$u(\partial\theta/\partial r)$	$w\partial M/\partial z$ $w\partial u/\partial z$	$u\partial M/\partial r$ $u\partial u/\partial r$
WC1	10⁴	10³	10⁴	Crowley	Crowley	Crowley	Crowley
WC2	2×10⁴	2×10⁴	2×10⁴	Do.	Do.	Do.	Do.
WC3	2×10⁴	2×10⁴	2×10⁴	Do.	Do.	Upstream	Do.
WC4	2×10⁴	2×10⁴	2×10⁴	Upstream	Do.	Do.	Do.

FIGURE 19.—Results from experiment WC2, cross section of tangential velocity at hour 96.
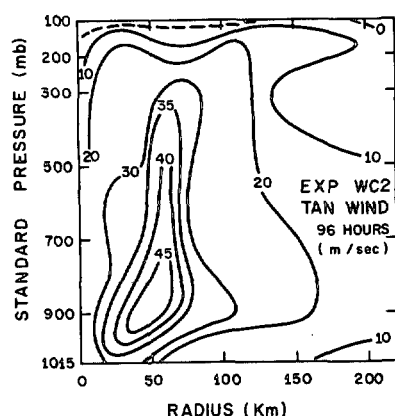

FIGURE 20.—Results from experiment WC3, cross section of tangential velocity at hour 96.

ternal and surface dissipation. While these "beneficial" aspects of upstream differencing are clearly fortuitous, their consistency in dozens of experiments demands rationalization. The material presented in section 4 is part of this rationalization and is really all that we have been able to obtain by analytical means.

While the remainder of this discussion is clearly heuristic, the implications of some of the material are interesting. They seem to lead to the conclusion that, with our present lack of knowledge concerning the interactions between the cumulus scale and the macroscale, the diffusive effects provided by upstream differencing are probably as good a representation of the statistical effect of the cumulus motions on the macroscale velocity fields as anything currently available. Such a conclusion, of course, only points to a high degree of ignorance with regard to an extremely important meteorological problem. It is by no means a solution to the problem.

We first point out that Riehl and Malkus (1961) estimated a vertical mixing coefficient for hurricane Daisy of the order of 100 m² sec⁻¹, which is also the order of the vertical coefficient of computational diffusion in the core of the storm (fig. 12). They also estimated a lateral mixing coefficient of the order of 10⁵ m² sec⁻¹ for the mature stage of hurricane Daisy and a value of less than 10⁴ m² sec⁻¹ for the immature stage. In comparison (fig. 13), the computational lateral mixing coefficient has the same temporal variation and, if anything, a somewhat smaller magnitude. If the Riehl-Malkus estimates are to be given any credence and if further we realize that the
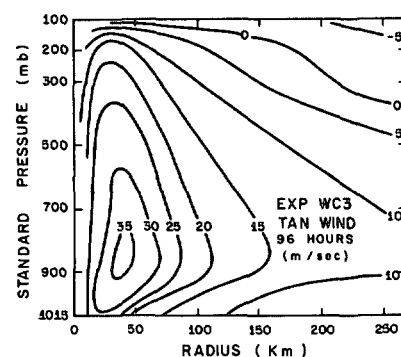
mixing coefficients must vary markedly in the horizontal because of the highly concentrated nature of the hurricane cumulonimbus pattern, realistic mixing coefficients (both for vertical and horizontal diffusion) must vary by orders of magnitude in both space and time. The computational coefficients have the proper spatial and temporal variations and, as we have seen, more or less the correct magnitude.

At this time, it is difficult to see how these coefficients could be improved upon through explicit representations. While equation (32) might be adequate for vertical mixing, a valid formulation for lateral mixing is not at all clear. Here, one is quickly led to think in terms of Smagorinsky's (1963) nonlinear eddy viscosity. However, Lilly (1961) in a discussion of the upstream method noted "Motions are damped, but rather selectively, and the general results appear to be very similar to those obtained using Smagorinsky's eddy friction form, although the physical significance is not clear."

If the results are, indeed, to be similar, the computing economics strongly favor the upstream method. In addition, the classical "hourglass" shape of the cumulonimbi strongly suggests that significant lateral mixing between the clouds and their environment is concentrated in the surface boundary layer and in the upper troposphere. For lateral mixing, the computational viscosity coefficient is given by

$$F_H = \frac{|u|\Delta r}{2}\left\{1 - \frac{|u|\Delta t}{\Delta r}\right\} \approx \frac{|u|\Delta r}{2}. \tag{62}$$

With the vertical variation of radial velocity typically found in real hurricanes and in models (fig. 16), the sense of the vertical variation of F_H will be similar to that sug-
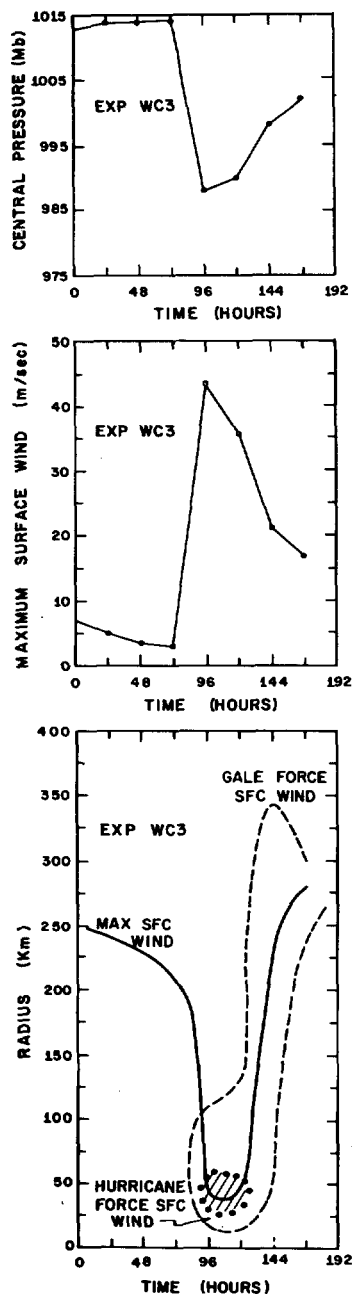
FIGURE 21.—Results from experiment WC3. Top, central pressure as a function of time; center, maximum surface wind as a function of time; bottom, radii of maximum surface wind and inner and outer limits of hurricane-force and gale-force winds at the surface.
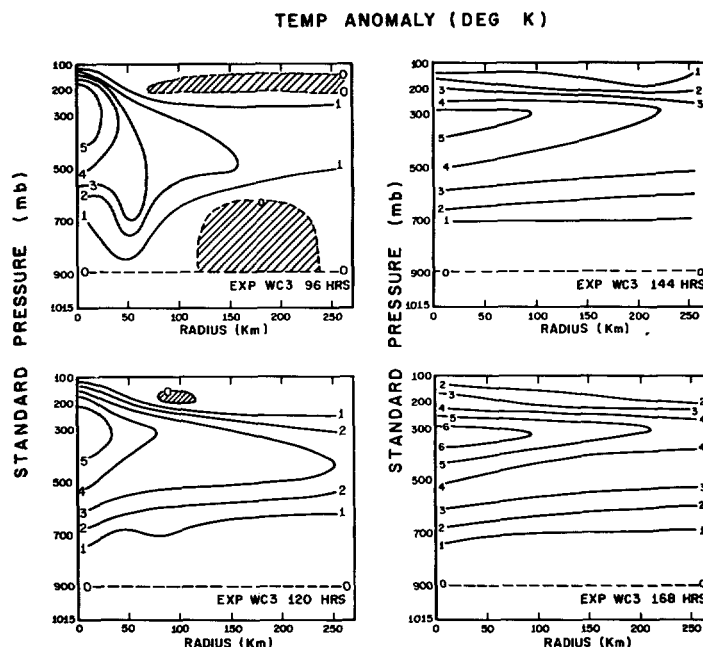

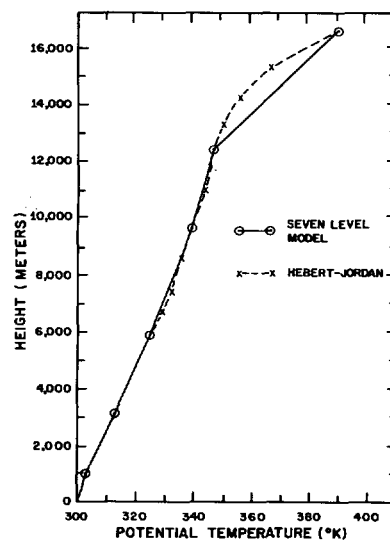FIGURE 22.—Results from experiment WC3, cross sections of temperature anomaly.

FIGURE 23.—Potential temperature as a function of height in the mean tropical atmosphere after Hebert and Jordan (1959). The dashed curve shows the structure when all data points are plotted. The solid curve shows the profile obtained when only the points that coincide with information levels of the seven-level model are plotted.

gested by the cloud shapes. Finally, it is noted that F_H is of the form of the product of an advecting velocity and a characteristic scale that is, in some sense, analogous to the type of relationship usually obtained from mixing length theory.

On the basis of these considerations, we have decided to retain the upstream method for the immediate future. It is interesting that a recent paper by Orville and Sloan (1970) makes similar comparisons between the upstream method and Crowley's scheme. Their calculations indicate that the two numerical schemes yield similar solutions for a cloud model, provided that the explicit diffusion coefficients used with the upstream method are increased when Crowley's method is applied. However, grid spacing (both in the horizontal and in the vertical) for this model is of the order of tens of meters. Hence, subgrid motions are "small" scale turbulence elements and not clouds as in the
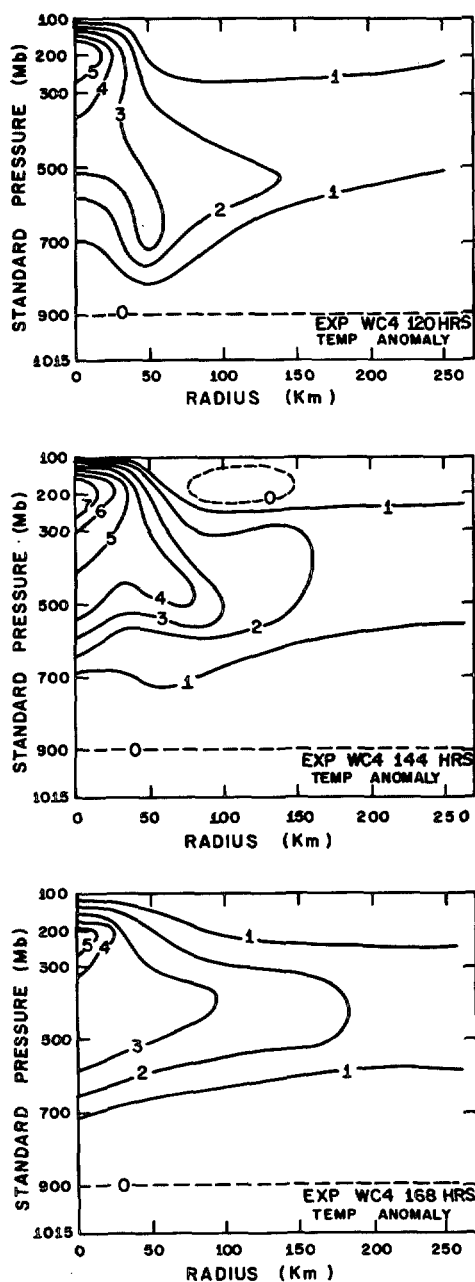
FIGURE 24.—Results from experiment WC4, cross sections of temperature anomaly.
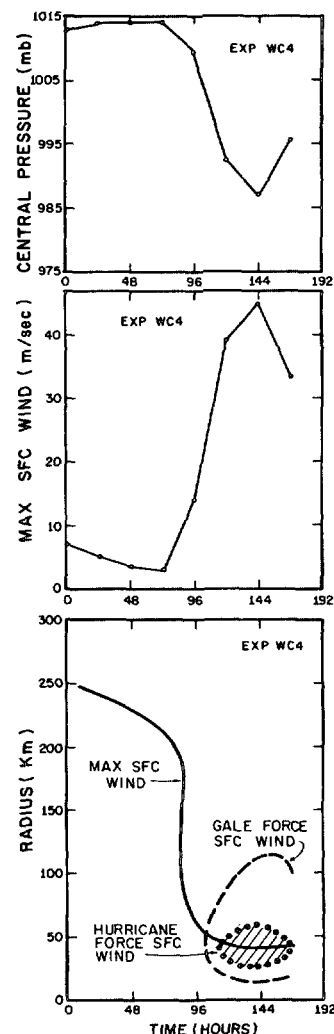

FIGURE 25.—Results from experiment WC4. Top, central pressure as a function of time; center, maximum surface wind as a function of time; bottom, radii of maximum surface wind and inner and outer limits of hurricane-force and gale-force winds at the surface.

hurricane model. This consideration probably explains the differences between the conclusions reached in this paper and those reached by Orville and Sloan (1970).

10. CONCLUSIONS

The new version of the model, which contains an explicit prediction of specific humidity and which simulates the evaporation of cloud material and subsequent enrichment of the macroscale humidity, yields more realistic rainfall rates and efficiencies than were obtained from older versions of the model (Rosenthal 1969a, 1969b). Recent empirical results (Hawkins and Rubsam 1968) that indi-

cate nonconvective precipitation to be a significant proportion of total precipitation are reproduced by the model. An experiment with extremely moist initial conditions (90 percent relative humidity at all grid points) shows that growth to the mature stage is more rapid in the moist environment but that the ultimate intensity of the storm is not greatly affected by the initial humidity distribution.

A sequence of experiments in which various advection terms were evaluated using Crowley's second-order advection form yielded results clearly inferior to those obtained with the upstream method. In an attempt to rationalize this surprising result, we found that the magnitude as well as the sense of the temporal and radial variations of the computational diffusion coefficients associated with the upstream method were much the same as deduced by Riehl and Malkus (1961) for the eddy viscosity coefficients of hurricane Daisy (1958).
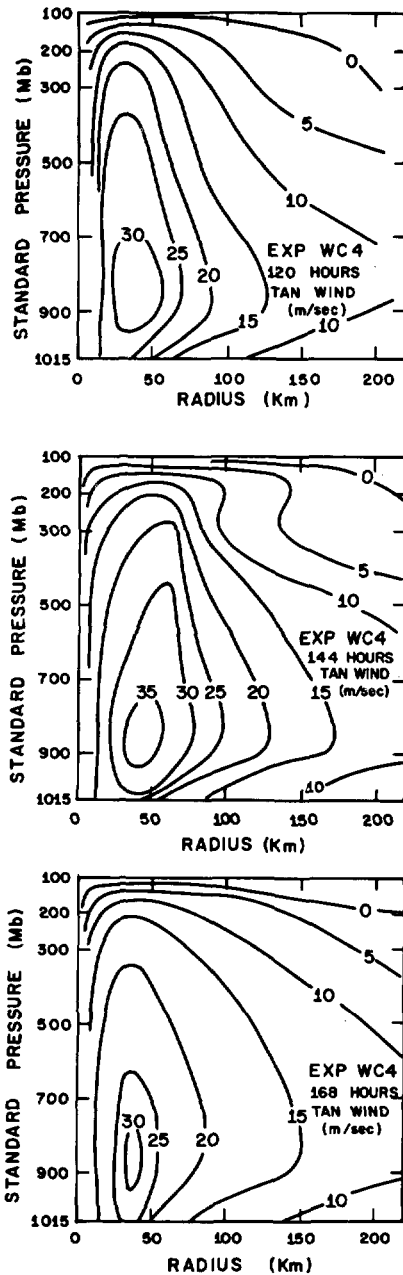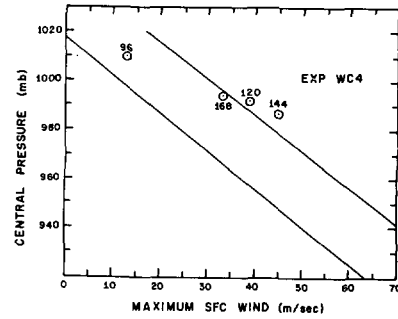
FIGURE 27.—Results from experiment WC4, central pressure plotted against maximum surface wind for hours 96, 120, 144, and 168. Parallel sloping lines are drawn to enclose most of Colón's (1963) empirical data points from a large number of tropical cyclones in various stages of life cycle.
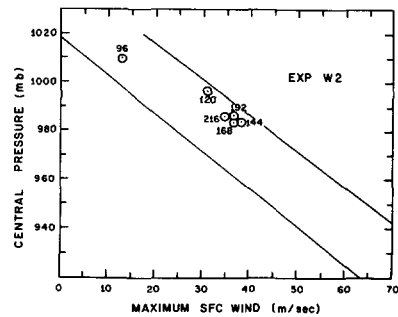

FIGURE 28.—Same as figure 27, but for experiment W2.

FIGURE 26.—Results from experiment WC4, cross sections of tangential wind.

APPENDIX

INITIALIZATION

A field of standard temperature, $\bar{\theta}=\bar{\theta}(z)$, is specified. These values are very nearly those of the mean hurricane season sounding (Hebert and Jordan 1959) and are listed in table 5.

The lower boundary condition, $\bar{\phi}_1=c_p(1015/1000)^{R/c_p}$, is adopted, and a set of standard $\bar{\phi}=\bar{\phi}(z)$ are calculated from the hydrostatic equation (40). A set of standard temperatures, $\bar{T}=\bar{T}(z)$, are calculated from (43). Equation (42) is then used to calculate standard pressures, $\bar{p}=\bar{p}(z)$.

Finally, the standard densities, $\bar{\rho}=\bar{\rho}(z)$, are obtained from $\bar{\rho}=\bar{p}/R\bar{T}$.

The initial temperature field is given by

$$T_{i,j}=\bar{T}_i+\bar{T}_*\left\{\cos\frac{\pi}{\hat{r}}\,r_j+1\right\}\sin\frac{\pi}{z_7}\,z_i$$

where $T_*=0.16°K$ and $\hat{r}=(J_{max}-1)\Delta r$. With the boundary condition $\phi_{7,j}=\bar{\phi}_7$, the hydrostatic equation, in the form $\partial\phi/\partial z=-g\theta/c_p T$ is integrated by the trapezoidal rule to obtain $\phi_{i,j}$ for $i=6, 5, \ldots, 1$. With T and ϕ initialized, initial values of θ are calculated from equation (43), the gradient wind equation is solved for the initial distribution of v, and M is then calculated from (44).

Initial conditions for specific humidity were established as follows. A base state relative humidity, very nearly equal to that of the mean hurricane season (Hebert and Jordan 1959), was specified as a function of height (see table 3 of the text). By use of the base state temperature and pressure, the relative humidity was converted to a specific humidity. The specific humidity at the initial instant was then assumed horizontally homogeneous and equal to the base state value.

COMPUTATIONAL CYCLE

For beginning a time step, M^r, u^r, w^r, θ^r, and q^r are

required. The superscript is the time index. Dependent variables are replaced with their new values as soon as they become available. The scheme is, therefore, semi-implicit, and the results depend on the order in which the calculations are carried out. Indeed, computational stability is dependent on the order of the calculations. The sequence given below has proved to be highly stable.

1. Calculate $\partial M/\partial t$ from equation (37). Use a forward time step to obtain M^{r+1}. Replace M^r with M^{r+1} for subsequent calculations.

2. Calculate B from equation (47) and H from (49).

3. Integrate equation (50) to obtain ϕ^r at level 1.

4. Calculate ϕ^r at the remaining levels by trapezoidal integration of the hydrostatic equation (40).

5. Calculate $\partial u/\partial t$ from equation (38). Use a forward time step to obtain u^{r+1}. Replace u^r with u^{r+1} for subsequent calculations.

6. Calculate w^{r+1} by trapezoidal integration of the continuity equation (41) and by use of the boundary condition (47). Replace w^r with w^{r+1} for subsequent calculations.

7. Use the method described in sections 2 and 3 to establish the convective adjustments of humidity and temperature.

8. Obtain a first estimate q^{r+1} from the method described in section 3. Include the convective adjustment.

9. Obtain a first estimate of θ^{r+1} from the thermodynamic equation (39). Include the convective adjustment.

10. Check for supersaturation. If supersaturation exists and if parcel ascent from the grid point is conditionally unstable, use the excess water vapor for a second convective adjustment. If supersaturation exists but parcel ascent is stable, condense water vapor at constant pressure until the temperature (humidity) has been raised (lowered) sufficiently to reach 100 percent relative humidity. The condensate is removed from the system as nonconvective precipitation.

11. Return to step (1) above for the forecast through the next time step.

GENERATION OF AVAILABLE POTENTIAL ENERGY

The generation of available potential energy was calculated from the approximate relationship

$$G=\frac{2\pi g^2}{c_p}\int_0^r\int_{z_1}^{z_7}\frac{T'\dot{H'}}{\overline{T}^2\overline{N}^2}\overline{\rho}rdrdz \tag{63}$$

where

$$\overline{(\quad)}=\frac{2\pi\int_0^{r*}(\quad)rdr}{\pi r^{*2}}, \tag{64}$$

$$r^*=400\ km, \tag{65}$$

$$(\quad)'=(\quad)-\overline{(\quad)}, \tag{66}$$

$$N^2=\frac{g}{\theta}\frac{\partial\theta}{\partial z}, \tag{67}$$

TABLE 5.—*Standard values of thermodynamic variables*

Level	Height	$\bar{\theta}$	$\bar{T}$	$\bar{p}$	$\bar{\rho}$
	(m)	(°K)	(°K)	(mb)	(ton m⁻³)
1	0	300	301. 3	1015. 0	1.174×10⁻³
2	1054	303	294. 1	900. 4	1.067×10⁻³
3	3187	313	282. 6	699. 4	0.862×10⁻³
4	5898	325	266. 5	499. 2	0.653×10⁻³
5	9697	340	240. 8	299. 2	0.433×10⁻³
6	12423	347	218. 9	199. 5	0.318×10⁻³
7	16621	391	203. 1	101. 1	0.173×10⁻³

and $\dot{H}$ is the total (convective plus large-scale) condensation heating per unit time and mass.

KINETIC ENERGY BUDGET

From the equations presented in section 5, we may derive the following expression for the kinetic energy tendency of the model storm:

$$\frac{\partial K}{\partial t}=T_E+I-D_V-D_H \tag{68}$$

where

$$K=2\pi\int_0^{r_b}\int_{z_1}^{z_7}\overline{\rho}r\left(\frac{u^2+v^2}{2}\right)dzdr, \tag{69}$$

$$T_E=-2\pi\int_0^{r_b}\int_{z_1}^{z_7}\overline{\rho}ru\theta\frac{\partial\phi}{\partial r}dzdr, \tag{70}$$

$$I=-2\pi\int_{z_1}^{z_7}\overline{\rho}r_bu_b\left(\frac{u_b^2+v_b^2}{2}\right)dz, \tag{71}$$

$$D_V=-2\pi\int_0^{r_b}\int_{z_1}^{z_7}r\left\{u\frac{\partial}{\partial z}\left(\overline{\rho}K_M^z\frac{\partial u}{\partial z}\right)+v\frac{\partial}{\partial z}\left(\overline{\rho}K_M^z\frac{\partial v}{\partial z}\right)\right\}dzdr, \tag{72}$$

and

$$D_H=-2\pi K_M^H\int_0^{r_b}\int_{z_1}^{z_7}\frac{\overline{\rho}}{r}\left\{u\frac{\partial}{\partial r}\left[r^3\frac{\partial}{\partial r}\left(\frac{u}{r}\right)\right]\right.$$
$$\left.+v\frac{\partial}{\partial r}\left[r^3\frac{\partial}{\partial r}\left(\frac{v}{r}\right)\right]\right\}dzdr. \tag{73}$$

By use of the boundary conditions given in the text (equations 56 and 57) and the distribution of K_M^z used for our experiments (table 2), the dissipation of kinetic energy by vertical mixing may be approximated by

$$D_V\approx2\pi\int_0^{r_b}r\overline{\rho}_1C_D|\mathbf{V}_1|^3dr. \tag{74}$$

For the sake of brevity, the dissipation due to lateral eddy viscosity is written in the form (73) rather than in a form that separates internal dissipation from dissipation at the lateral boundary.

If we average equation (68) over a time interval $\hat{t}$, we obtain

$$\frac{\partial\bar{K}}{\partial t}=\frac{K^{(t+\hat{t})}-K^{(t)}}{\hat{t}}=\bar{T}_E+\bar{I}-\bar{D}_V-\bar{D}_H, \tag{75}$$

where

$$(\bar{\ })=\frac{1}{\hat{t}}\int_t^{t+\hat{t}}(\quad)dt'. \tag{76}$$

The kinetic energy budgets discussed in the text are based on 12-hr averages with computations performed at 12-hr intervals. All terms in equation (75) may be evaluated directly from the output of the model. In general, there will be a significant residual due to truncation error. It is this residual that is plotted on figure 11.

KINETIC ENERGY DISSIPATION BY UPSTREAM DIFFERENCING

The dissipation due to differencing $w(\partial M/\partial z)$ and $w(\partial u/\partial z)$ by the upstream method may be written as

$$C_V = -2\pi \int_0^{r_b} \int_{z_1}^{z_7} \bar{\rho} r F_z \left\{ u\frac{\partial^2 u}{\partial z^2} + v\frac{\partial^2 v}{\partial z^2} \right\} dz\,dr \qquad (77)$$

where the pseudoviscosity coefficient is given by

$$F_z = \tfrac{1}{2}|w|\Delta z \left\{ 1 - \frac{|w|\Delta t}{\Delta z} \right\}. \qquad (78)$$

The dissipation due to upstream differencing of $u(\partial M/\partial r)$ and $u(\partial u/\partial r)$ is

$$C_H = -2\pi \int_0^{r_b} \int_{z_1}^{z_7} \bar{\rho} F_H \left\{ v\frac{\partial^2 M}{\partial r^2} + ru\frac{\partial^2 u}{\partial r^2} \right\} dr\,dz \qquad (79)$$

where

$$F_H = \tfrac{1}{2}|u|\Delta r \left\{ 1 - \frac{|u|\Delta t}{\Delta r} \right\}. \qquad (80)$$

ACKNOWLEDGMENTS

REFERENCES

Anthes, Richard A., and Johnson, Donald R., "Generation of Available Potential Energy in Hurricane Hilda (1964)," *Monthly Weather Review*, Vol. 96, No. 5, May 1968, pp. 291–302.

Charney, Jule G., and Eliassen, Arnt, "On the Growth of the Hurricane Depression," *Journal of the Atmospheric Sciences*, Vol. 21, No. 1, Jan. 1964, pp. 68–75.

Colón, José A., "On the Evolution of the Wind Field During the Life Cycle of Tropical Cyclones," *National Hurricane Research Project Report* No. 65, U.S. Department of Commerce, National Hurricane Research Laboratory, Miami, Fla., Nov. 1963, 36 pp.

Crowley, W. P., "Numerical Advection Experiments," *Monthly Weather Review*, Vol. 96, No. 1, Jan. 1968, pp. 1–11.

Estoque, Mariano A., "Vertical Mixing Due to Penetrative Convection," *Journal of the Atmospheric Sciences*, Vol. 25, No. 6, Nov. 1968, pp. 1046–1051.

Gray, William M., "The Mutual Variation of Wind, Shear, and Baroclinicity in the Cumulus Convective Atmosphere of the Hurricane," *Monthly Weather Review*, Vol. 95, No. 2, Feb. 1967, pp. 55–73.

Hawkins, Harry F., and Rubsam, Daryl T., "Hurricane Hilda, 1964: II. Structure and Budgets of the Hurricane on October 1, 1964," *Monthly Weather Review*, Vol. 96, No. 9, Sept. 1968, pp. 617–636.

Hebert, Paul J., and Jordan, C. L., "Mean Soundings for the Gulf of Mexico Area," *National Hurricane Research Project Report* No. 30, U.S. Department of Commerce, National Hurricane Research Laboratory, Miami, Fla., Apr. 1959, 10 pp.

Kuo, H. L., "On Formation and Intensification of Tropical Cyclones Through Latent Heat Release by Cumulus Convection," *Journal of the Atmospheric Sciences*, Vol. 22, No. 1, Jan. 1965, pp. 40–63.

Lilly, D. K., "A Proposed Staggered-Grid System for Numerical Integration of Dynamic Equations," *Monthly Weather Review*, Vol. 89, No. 3, Mar. 1961, pp. 59–65.

Matsuno, Taroh, "Numerical Integrations of the Primitive Equations by a Simulated Backward Difference Method," *Journal of the Meteorological Society of Japan*, Ser. 2, Vol. 44, No. 1, Feb. 1966, pp. 76–84.

Miller, Banner I., "On the Momentum and Energy Balance of Hurricane Helene (1958)," *National Hurricane Research Project Report* No. 53, U.S. Department of Commerce, National Hurricane Research Laboratory, Miami, Fla., Apr. 1962, 19 pp.

Molenkamp, Charles R., "Accuracy of Finite-Difference Methods Applied to the Advection Equation," *Journal of Applied Meteorology*, Vol. 7, No. 2, Apr. 1968, pp. 160–167.

Ooyama, Katsuyuki, "Numerical Simulation of the Life Cycle of Tropical Cyclones," *Journal of the Atmospheric Sciences*, Vol. 26, No. 1, Jan. 1969, pp. 3–40.

Orville, H. D., and Sloan, L. J., "Effects of Higher Order Advection Techniques on a Numerical Cloud Model," *Monthly Weather Review*, Vol. 98, No. 1, Jan. 1970, pp. 7–13.

Palmén, E., and Riehl, Herbert, "Budget of Angular Momentum and Energy in Tropical Cyclones," *Journal of Meteorology*, Vol. 14, No. 2, Apr. 1957, pp. 150–159.

Riehl, Herbert, *Tropical Meteorology*, McGraw-Hill Book Co., Inc., New York, 1954, 392 pp.

Riehl, Herbert, and Malkus, Joanne S., "Some Aspects of Hurricane Daisy, 1958," *Tellus*, Vol. 13, No. 2, May 1961, pp. 181–213.

Rosenthal, Stanley L., "Numerical Experiments With a Multilevel Primitive Equation Model Designed to Simulate the Development of Tropical Cyclones, Experiment I," *ESSA Technical Memorandum* ERLTM–NHRL 82, U.S. Department of Commerce, National Hurricane Research Laboratory, Miami, Fla., Jan. 1969a, 36 pp.

Rosenthal, Stanley L., "Experiments With a Numerical Model of Tropical Cyclone Development. Some Effects of Radial Resolution," *ESSA Technical Memorandum* ERLTM–NHRL 87, U.S. Department of Commerce, National Hurricane Research Laboratory, Miami, Fla., Aug. 1969b, 47 pp.

Smagorinsky, J., "General Circulation Experiments With the Primitive Equations: I. The Basic Experiment," *Monthly Weather Review*, Vol. 91, No. 3, Mar. 1963, pp. 99–164.

Yamasaki, Masanori, "A Tropical Cyclone Model With Parameterized Vertical Partition of Released Latent Heat," *Journal of the Meteorological Society of Japan*, Vol. 46, No. 3, June 1968a, pp. 202–214.

Yamasaki, Masanori, "Detailed Analysis of a Tropical Cyclone Simulated With a 13-Layer Model," *Papers in Meteorology and Geophysics*, Vol. 19, No. 4, Dec. 1968b, pp. 559–585.